

## Export of Ice Sheet Meltwater from Upernavik Fjord, West Greenland

MORVEN MUILWIJK,<sup>a,b</sup> FIAMMA STRANEO,<sup>c,a</sup> DONALD A. SLATER,<sup>c,d,e</sup> LARS H. SMEDSRUD,<sup>a,b</sup> JAMES HOLTE,<sup>c</sup> MICHAEL WOOD,<sup>f</sup> CAMILLA S. ANDRESEN,<sup>g</sup> AND BEN HARDEN<sup>h</sup>

<sup>a</sup> *Geophysical Institute, University of Bergen, Bergen, Norway*

<sup>b</sup> *Bjerknes Centre for Climate Research, Bergen, Norway*

<sup>c</sup> *Scripps Institution of Oceanography, University of California, San Diego, La Jolla, California*

<sup>d</sup> *School of Geography and Sustainable Development, University of St. Andrews, St Andrews, United Kingdom*

<sup>e</sup> *School of Geosciences, University of Edinburgh, Edinburgh, United Kingdom*

<sup>f</sup> *Jet Propulsion Laboratory, California Institute of Technology, Pasadena, California*

<sup>g</sup> *Department of Glaciology and Climate, Geological Survey of Denmark and Greenland, København, Denmark*

<sup>h</sup> *Sea Education Association, Woods Hole, Massachusetts*

(Manuscript received 16 April 2021, in final form 10 December 2021)

**ABSTRACT:** Meltwater from Greenland is an important freshwater source for the North Atlantic Ocean, released into the ocean at the head of fjords in the form of runoff, submarine melt, and icebergs. The meltwater release gives rise to complex in-fjord transformations that result in its dilution through mixing with other water masses. The transformed waters, which contain the meltwater, are exported from the fjords as a new water mass Glacially Modified Water (GMW). Here we use summer hydrographic data collected from 2013 to 2019 in Upernavik, a major glacial fjord in northwest Greenland, to describe the water masses that flow into the fjord from the shelf and the exported GMWs. Using an optimum multi-parameter technique across multiple years we then show that GMW is composed of  $57.8\% \pm 8.1\%$  Atlantic Water (AW),  $41.0\% \pm 8.3\%$  Polar Water (PW),  $1.0\% \pm 0.1\%$  subglacial discharge, and  $0.2\% \pm 0.2\%$  submarine meltwater. We show that the GMW fractional composition cannot be described by buoyant plume theory alone since it includes lateral mixing within the upper layers of the fjord not accounted for by buoyant plume dynamics. Consistent with its composition, we find that changes in GMW properties reflect changes in the AW and PW source waters. Using the obtained dilution ratios, this study suggests that the exchange across the fjord mouth during summer is on the order of 50 mSv ( $1 \text{ Sv} \equiv 10^6 \text{ m}^3 \text{ s}^{-1}$ ) (compared to a freshwater input of 0.5 mSv). This study provides a first-order parameterization for the exchange at the mouth of glacial fjords for large-scale ocean models.

**KEYWORDS:** Ocean; Arctic; Atlantic Ocean; Glaciers; Ice sheets; Buoyancy; Entrainment; In situ oceanic observations; Annual variations


### 1. Introduction

During the last three decades, the Greenland Ice Sheet has been losing mass at an accelerating rate, from  $-26 \pm 27 \text{ Gt yr}^{-1}$  between 1992 and 1997 to  $-244 \pm 28 \text{ Gt yr}^{-1}$  between 2012 and 2017 (Shepherd et al. 2020), and is projected to continue to do so (Shepherd et al. 2020; Goelzer et al. 2020). The ice loss from Greenland translates into an increased freshwater flux into the ocean, which contributes to global sea level rise, and has the potential to impact the regional and large-scale ocean circulation, including the Atlantic meridional overturning circulation (AMOC; Bamber et al. 2012, 2018; Böning et al. 2016; Frajka-Williams et al. 2016; Shepherd et al. 2020; Le Bras et al. 2021; Caesar et al. 2021). Recent modeling studies have sought to evaluate the impact of this increased freshwater discharge (now or in the future), but since the models do not resolve the fjords or glacier/ocean exchanges, the excess discharge is typically imposed as a surface or upper layer freshwater flux around Greenland's perimeter (Swingedouw

et al. 2013; Dukhovskoy et al. 2016). Recent observations, however, show that Greenland's freshwater is rapidly diluted within hundreds of meters from the ice margins and exported from fjords as part of a more complex fjord/shelf exchange whose volume fluxes in and out of the fjord are over an order of magnitude greater than the pure freshwater flux alone (Beard et al. 2015, 2017, 2018; Mortensen et al. 2020).

Greenland's freshwater discharge occurs at the ice sheet-ocean boundary and consists of both liquid freshwater and solid ice (Bamber et al. 2018). It is released at the head of fjords through three different processes: seasonal runoff from surface melt, calved icebergs, and submarine melting of marine-terminating glaciers and ice shelves. Van den Broeke et al. (2016) estimated that on average, during 1991–2015, surface melt runoff amounted to 11 mSv ( $1 \text{ Sv} \equiv 10^6 \text{ m}^3 \text{ s}^{-1}$ ;  $363 \text{ Gt yr}^{-1}$ ), while the sum of solid ice discharge and submarine melting amounted to 15 mSv ( $477 \text{ Gt yr}^{-1}$ ). While it varies depending over the period considered, the increase in freshwater discharge is partitioned roughly equally between an increase in runoff or an increase in ice discharge (Enderlin et al. 2014; Mougnot et al. 2019).

In the case of marine-terminating glaciers, which account for the drainage of 88% of the Greenland ice sheet area (Rignot et al. 2012), most of the runoff enters the ocean at the glacier's base as subglacial discharge (SGD) often hundreds

 Denotes content that is immediately available upon publication as open access.

Corresponding author: Morven Muilwijk, morven@uib.no

DOI: 10.1175/JPO-D-21-0084.1

© 2022 American Meteorological Society. For information regarding reuse of this content and general copyright information, consult the AMS Copyright Policy ([www.ametsoc.org/PUBSReuseLicenses](http://www.ametsoc.org/PUBSReuseLicenses)).

of meters beneath the surface (Straneo and Cenedese 2015). This release of freshwater at depth gives rise to turbulent upwelling, entrainment of deep water masses, and a generally complex transformation of ambient water masses that provide the heat for melting ice and/or are made lighter through the mixing with the meltwater released. Thus, at least in summer, the release of SGD and submarine melt are tightly connected (Slater et al. 2015, 2016). In addition, icebergs melt in the fjords as they transit from the glacier to the open ocean, releasing much of this meltwater at depth (Moon et al. 2018). The liquid export from the fjord (excluding the icebergs), is therefore a mixture of modified ambient waters, iceberg melt, SGD and glacier melt known as Glacially Modified Water (GMW) (Straneo et al. 2011; Beaird et al. 2015, 2018; Moon et al. 2018; Mortensen et al. 2020). Noble gas measurements from Greenland's glacial fjords have confirmed that GMW consists of strongly diluted glacier and iceberg meltwater and SGD (less than 5% each), upwelled deep fjord waters, and lighter waters present on the continental shelf (Beaird et al. 2015, 2018). In particular, these studies show that Greenland's meltwater is not exported as a surface freshwater flux but instead as GMW distributed over the upper 100–200 m. For Sermilik Fjord (southeast Greenland) where velocity measurements exist, furthermore, they suggest that the exchange flow at the mouth of the fjord is approximately 30 times larger than the meltwater and runoff discharge into the fjord (Beaird et al. 2018). This transformation, dilution, and fjord–shelf exchange must be considered when formulating boundary conditions for ocean models (Böning et al. 2016; Dukhovskoy et al. 2019), which might, for example, consist of mass removal at depth and mass input closer to the fjord surface. Currently, however, observations of the GMW properties and volumes are limited, and there is no simple parameterization that can take the glacial and oceanic inputs and transform these into ocean model boundary conditions.

Here, we address this gap by deriving GMW properties using (summer) hydrographic data collected in one major Greenland glacial fjord over multiple years. Specifically, we identify GMW by comparing the shelf and fjord water masses. Furthermore, we investigate how the GMW properties change in time as a function of the glacial inputs and the properties of the water masses present on the shelf. Our analysis is compared to estimates of GMW derived from buoyant plume theory. Finally, we discuss how results from this study can be generalized for other glacial fjords.

This manuscript is organized as follows: in section 2 we describe the study region; in section 3 we document the datasets we have used, define the water masses and outline our methods, including GMW fractional composition analysis and plume model theory; in section 4 we present the hydrographic properties of a major Greenland fjord, and the results stemming from our GMW fractional composition analysis and the investigation of the relationship between the shelf and fjord water masses; in section 5 we discuss the implications of this work in a broader context before we summarize our findings in section 6. A sensitivity study and the uncertainties of our results are documented in the appendix.

## 2. Study region and oceanographic setting

### a. Regional oceanographic setting

This study focuses on the Upernavik Isfjord system, a large fjord in northwest Greenland (72.54°N, 55°W) fed by five large glaciers. The fjord discharges into Baffin Bay (Fig. 1), where the hydrography is dominated by relatively warm and saline Atlantic Water (AW) at depth and colder and fresher Polar Water (PW) on top (Münchow et al. 2015; Wood et al. 2021). The AW and PW enter Baffin in the south, through Davis Strait, and flow northward on the eastern side as the West Greenland Slope Current and West Greenland Current, respectively (Fig. 1; Curry et al. 2011; Johnson et al. 2011; Münchow et al. 2015; Heuzé et al. 2016; Rysgaard et al. 2020; Vermassen et al. 2019).

### b. Upernavik fjord

Upernavik fjord is approximately 60 km long and 5–7 km wide. The Rossby radius in this region is approximately the same as the width of the fjord (Nurser and Bacon 2014), so we expect the circulation to be weakly geostrophic but do not expect opposing flows on each side of the fjord. Near the fjord's head, we find the Upernavik Isstrøm (Sermeq) ice stream, which consists of five glaciers (Fig. 2). The fjord bathymetry (Fig. 2) has been mapped using sonar during a cruise in 2013 led by the Geological Survey of Denmark (Andresen et al. 2014) and as part of NASA's Oceans Melting Greenland ship survey 2016 (OMG Mission 2020). These data have been included in the BedMachine Version 3 topographic dataset (Morlighem et al. 2017) used in this study. The fjord is characterized by steep walls and a flat bottom at ~900-m depth (Vermassen et al. 2019). Near the head of the fjord water, local fishermen report water depths of 600–800 m (Andresen et al. 2014), but due to ice conditions, no bathymetric data were collected near the glacier fronts. In 2019 an Airborne Expendable Conductivity, Temperature and Depth (AXCTD) deployed near the front of Upernavik Isstrøm N (Fig. 2) suggested the water depth may be as large as 1000 m, indicating high uncertainty about the water depth near the glaciers and the glacier grounding depths. Based on the bathymetry available, the deepest channel from the continental shelf to the Upernavik is at least 600 m deep.

## 3. Methods

### a. Datasets

We use data from yearly (summer) occupations from 2013 to 2019, except for 2014, from which we have no data (Table 1; Straneo and Muilwijk 2021). For the years 2013, 2015, and 2016 data were collected by ship. In 2013, temperature, conductivity, and pressure data in and around Upernavik were collected by Sea-Bird SBE19plus and RBR Concerto CTDs from the research vessel R/V *Porsild*. Ship CTD data from 2015 to 2016 was provided by the NASA campaign Oceans Melting Greenland (OMG Mission 2020), and conducted by the M/V *Cape Race* and the S/Y *Ivilia*, both commercial vessels equipped with an AML Oceanographic

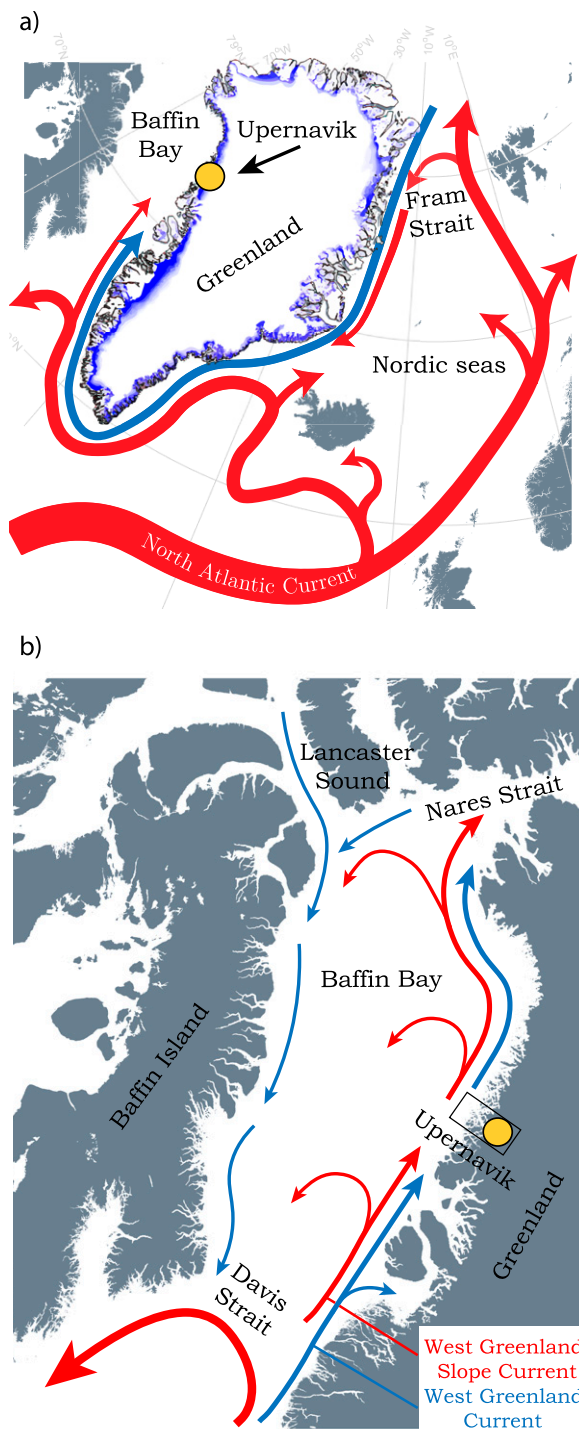


FIG. 1. Schematic of the large-scale ocean circulation in (a) the North Atlantic and Nordic Seas [adapted from Straneo et al. (2013) and Perner et al. (2019)] and (b) Baffin Bay (adapted from Curry et al. 2011). The North Atlantic Current brings warm and saline Atlantic Water (red arrows) northward and onto the Greenland shelves, and the East Greenland Current brings colder fresher Polar Water (blue arrows) southward from the Polar Seas. Our case study fjord “Upernavik” is marked in yellow.

Minos X CTD. For 2016–19 we use profiles collected from AXCTD probes from the OMG project (Fenty et al. 2016), hereafter referred to as “OMG-AXCTD.” Table 1 gives an overview of all hydrographic profiles used in this study, and profile locations are shown in Fig. 2. The year 2013 is the only year when we have no profile from the shelf, except for some shallow seal temperature profiles retrieved from *World Ocean Atlas 2018* (WOA18; Locarnini et al. 2018). Therefore, the shelf conditions for 2013 are based on a WOA18 (Locarnini et al. 2018) climatological profile, which has been adjusted linearly in temperature and salinity so that the AW properties at sill depth match the AW properties in the fjord.

We use the TEOS10 Gibbs-SeaWater Oceanographic Toolbox (McDougall and Barker 2011) to convert the conductivity profiles into Absolute Salinity ( $S_A$ ), temperature into Conservative Temperature (CT), and pressure into depth. We hereafter refer to Conservative Temperature as temperature and Absolute Salinity as salinity. OMG-AXCTD temperature and salinity data were edited with the removal of occasional noisy surface data, binned in regular depth intervals, and smoothed using a low-pass filter. All AXCTD profiles have undergone careful manual quality control. Their vertical coordinates (depth) are based on a constant fall rate and are therefore somewhat less accurate than data collected from a ship-based CTD, which measure pressure directly.

To investigate regional AW and PW hydrographic variability, we use the Estimating the Climate and Circulation of the Ocean (ECCO) global ocean and sea ice state estimate Version 4, Release 3 for the period 2010–17 (Forget et al. 2015). Khazendar et al. (2019) compare ECCO temperatures with observations from the Davis Strait mooring array (Curry et al. 2014) for 2009–18 and show that the model captures the timing and magnitude of the seasonal and interannual variations in Baffin Bay well. SGD estimates are from Slater et al. (2019): first, glacier hydrological catchments are delineated by routing water according to the hydropotential as defined by the subglacial topography and ice thickness, and second, surface melting over the catchment is estimated using the regional climate model RACMO (Noël et al. 2018).

#### b. Water mass definitions

To define the fjord water masses, we build on a generalized description of the transformation and circulation of water masses in a typical Greenland fjord, as shown in Fig. 3. We assume that there exists a deep (dense) water mass at sill depth, which also reaches the glacier grounding line, and a lighter water mass on top, which is also found on the shelf. In addition, there are two glacial water inputs: subglacial discharge (SGD) from surface runoff and submarine meltwater (SMW) from basal melt at the glacier terminus and iceberg melt (Fig. 3a). According to this generalized description [see also review by Straneo and Cenedese (2015)], the combined SGD and SMW drive turbulent plumes (Carroll et al. 2015; Slater et al. 2016), which cause the upwelling of deep fjord waters. This upwelling likely acts to precondition the fjord for renewal of deep waters (Carroll et al. 2018). Because of their relatively warm temperatures, both the deep

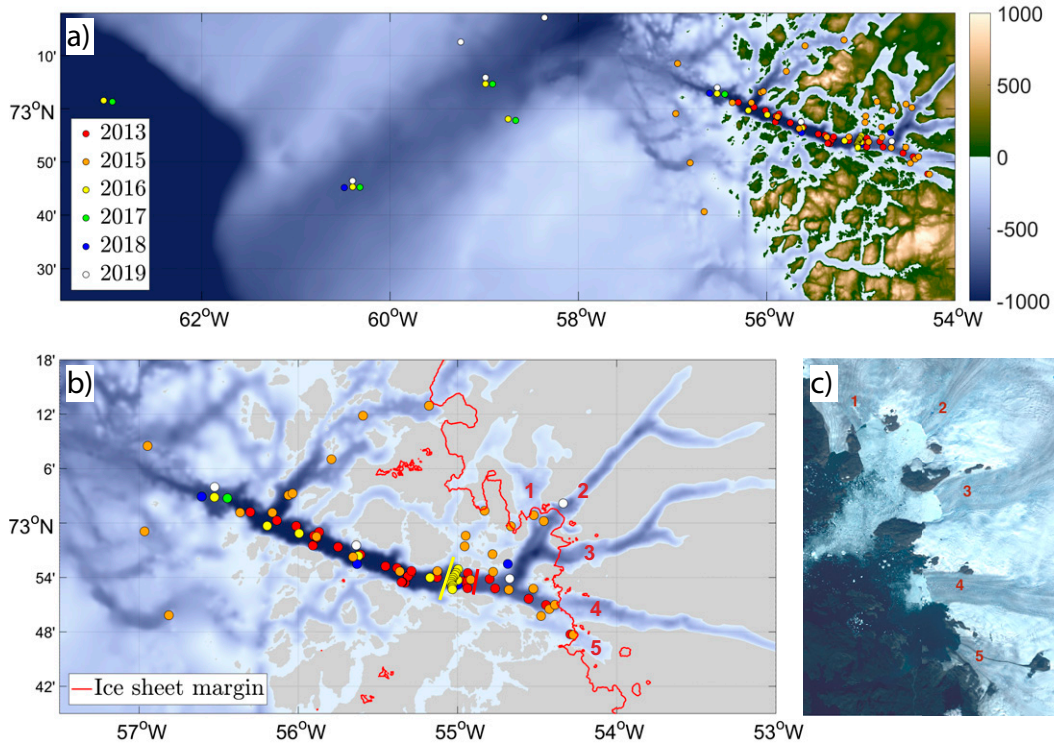


FIG. 2. Bathymetric map of the Upernavik fjord (box in Fig. 1) showing locations of hydrographic profiles obtained by ship (2013, 2015, and 2016) and by airborne AXCTD 2016–19 (OMG Mission 2020), referred to as “OMG-AXCTD.” (a) Both the shelf region (defined west of 56.2°W) and the deep fjord are shown; (b) a zoom in on the fjord only. Bathymetry and subglacial topography are based on BedMachine Version 3 (Morlighem et al. 2017). (c) Landsat satellite image (2020) of the five marine-terminating glaciers in the Upernavik Fjord system: 1) Unnamed, 2) Upernavik Isstrøm N, 3) Upernavik Isstrøm C (Sermeq), 4) Upernavik Isstrøm S, and 5) Upernavik Isstrøm SS (Bjørk et al. 2015). The across-fjord section for 2013 is marked with a red line, and the across-fjord section for 2016 is marked with a yellow line.

and lighter water masses can drive melting of the glaciers and icebergs, and are thus mixed with SGD and SMW (Straneo et al. 2011). Explicitly, the deep fjord waters are modified by glacier/iceberg interaction; rise as a result of the added melt-water and reach neutral buoyancy in the upper layer of the fjord. Here these waters are further transformed via lateral mixing with water masses present in the fjord’s upper layers as a result of shelf/fjord exchange (De Andrés et al. 2020). The resulting modified water mass is what is exported from the fjord and is what is known as GMW. It is made up of four

TABLE 1. Overview of hydrographic profile data for Upernavik 2013–19. The number of profiles on the shelf are given in parentheses and the others are taken inside the fjord.

Year	Period	Platform	Profiles
2013	31 Aug–2 Sep	R/V <i>Porsild</i>	29 (0)
2015	16 Sep–17 Sep	M/V <i>Cape Race</i>	11 (1)
2016	15 Sep–17 Sep	S/Y <i>Ivilia</i>	14
2016	24 Sep	Gulfstream III AXCTD	2 (3)
2017	19 Oct	C-130 Hercules AXCTD	1 (4)
2018	5 Sep	Basler BT-67 AXCTD	4 (1)
2019	30 Aug	Basler BT-67 AXCTD	3 (4)

different water masses: the fjord’s deep and upper water masses, which are both sourced from the shelf region, and two freshwater sources due to glacial inputs, SGD and SMW. Following this, and consistent with the findings of Beaird et al. (2015) and Beaird et al. (2018), the properties of GMW are a combination of properties from four water masses alone.

To identify GMW from fjord hydrography we propose the following framework. First, we assume that the properties of water masses in the fjord are mainly controlled by the exchange with the shelf and interaction with the glaciers while the air–sea surface fluxes have a negligible impact. Surface fluxes would likely be confined to a thin surface layer, which we argue should be excluded from this type of analysis. The effect of sea ice growth and melt is also limited to the surface, and therefore, not expected to have a large effect on deeper water masses. Wind presumably plays a role in the fjord renewal and hence in the GMW formation (e.g., Jackson et al. 2014, 2018) and as such its effect is implicitly included in GMW formulation. Interannual variations in wind forcing, presumably, may affect the GMW composition but here we assume that to first order this variability can be ignored. Finally, we neglect variability in the

across- and along-fjord direction. It will be seen from our results that the variability in properties within the fjord is much smaller than the contrast in properties between the fjord and shelf, enabling us to define GMW based on differences between the fjord and shelf, without worrying about where in the fjord properties are measured.

By comparing water masses on the shelf with water masses in the fjord [similarly to what was done in Straneo et al. (2012)], we identify both the inflowing deep waters and the shallower outflowing GMW (Fig. 3). Our method relies on identifying a set of appropriate profiles from the fjord and the shelf for the same period. We then calculate a temperature and salinity anomaly on isopycnals of the fjord profiles relative to the mean shelf profiles ( $\Delta CT$  and  $\Delta S_A$ ). In other words,  $\Delta CT$  and  $\Delta S_A$  are the “along-isopycnal” differences between the fjord and shelf. The procedure is summarized in Fig. 3b for a generic fjord in Greenland where the shelf is characterized by a cold and light water mass overlaying a warmer and denser water mass. The fjord deep water, which comes over the sill and is found at the glacier’s grounding line depth, is defined as a zero anomaly in temperature and salinity from the shelf to the fjord. GMW is then defined as the layer with maximum temperature and salinity anomalies. This description of water masses is consistent with the fact that at intermediate depths (~100–300 m), Greenland’s fjords with large marine-terminating glaciers are characterized by a layer with higher temperature and salinity relative to fresher and colder water of the same density on the shelf (Fig. 3b). This is a direct result of the upwelling of warm and salty deep fjord water driven by the SMW/SGD plume near the glacial front (Slater et al. 2016). The lower boundary of the GMW layer is therefore defined as the depth where  $\Delta CT$  and  $\Delta S_A$  reach zero below the maximum (Fig. 3). The upper boundary of the GMW is defined as where  $\Delta CT$  and  $\Delta S_A$  first reach zero above the maximum of  $\Delta CT/\Delta S_A$  unless this is shallower than 50 m, which we define as the surface layer depth. If the boundary is shallower than 50 m, we define the upper boundary of GMW to be 50 m to exclude any surface processes. We note that this GMW definition is preferred to one based on fixed vertical coordinates. It allows the GMW layer’s depth to vary in time, for example, due to varying SGD or inflowing deep water from year to year. Also, a fixed water mass definition based on temperature, salinity, and density will not allow for interannual variability of the source water masses which make up this mixture. We tested our definition in an extensive experiment where we compared our result to results from nine different pairs of fixed vertical coordinates (Table A1). Overall, our varying depth definition is the only definition that can properly capture the GMW and its variability.

In Greenland’s major glacial fjords, the deep fjord waters are often of Atlantic origin (AW), while the upper-layer waters are often of Arctic origin (PW; Straneo et al. 2012). In Upernavik fjord, the deep waters are believed to originate from the south (Vermassen et al. 2019) and enter the area through a deep cross-shelf trough (Fig. 2) and we therefore identify these waters as AW. This deep fjord water flows unmodified from the shelf at sill depth. The lighter, upper

layer on the shelf is defined as PW. In this study we are particularly interested in the PW layer that has the same density as the GMW, and therefore only focus on the PW bounded by the same isopycnals that defines the GMW. Likely, PW extends below and above this layer, but we assume that the relevant water mass is the one that will mix along isopycnals with the GMW.

### c. Properties of SMW and SGD

SMW is the fresh meltwater resulting from submarine melting of glaciers and icebergs and in mixing processes is characterized by a very low “effective” temperature due to the latent heat that has to be supplied to melt the ice (Jenkins 1999; Straneo et al. 2011). Assuming conservation of mass and heat, the temperature and salinity characteristics of an ambient/SMW mixture will fall along a continuous line (Gade 1979) in temperature/salinity space (Straneo et al. 2011). The line joins the ambient water mass (AW in our case) with the effective temperature ( $\theta_{ef}$ ) of the ice, which is given by Jenkins (1999):

$$T_{SMW} = \theta_{ef} = \theta_f - \frac{L}{C_p} - \frac{C_i}{C_p}(\theta_f - \theta_i) = -90^\circ\text{C}, \quad (1)$$

where  $\theta_f$  is the freezing temperature of seawater,  $L$  is the latent heat of fusion for ice ( $3.3 \times 10^5 \text{ J kg}^{-1}$ ),  $C_i$  ( $2100 \text{ J kg}^{-1}$ ) and  $C_p$  ( $3980 \text{ J kg}^{-1}$ ) are the specific heat capacities of ice and water, respectively, and  $\theta_i$  is the actual ice temperature. Following this, we use  $T_{SMW} = -90^\circ\text{C}$  and  $S_{SMW} = 0 \text{ g kg}^{-1}$ .

SGD is also cold and fresh and represents the subglacial discharge of runoff (i.e., the runoff that exits at the base of the glacier). If a water mixture consists of only ambient water and SGD, it falls along a straight line in temperature/salinity space, which connects the ambient water properties with the discharge properties ( $S_{SGD} = 0 \text{ g kg}^{-1}$  and  $T_{SGD} = 0^\circ\text{C}$ ).

### d. GMW composition analysis

This study aims to study the composition of the GMW and how this varies over time concerning the source waters. To achieve this, we use a technique based on the optimum multi-parameter analysis (OMP) method (Tomczak and Large 1989), which was also used by Beaird et al. (2015) and Beaird et al. (2018). The OMP is based on a set of linear mixing equations that connect water properties (temperature, salinity, helium, etc.) to a set number of water mass endmembers. For each of the properties a linear mixing equation is written such that the mixture water mass is given as a sum of fractions of each of the water mass endmembers multiplied by the value of the property for each water mass endmember. For example, if the property is temperature and there are four water masses (being AW, PW, SGD, and SMW), the mixing equation is

$$T_{GMW} = \alpha T_{AW} + \beta T_{PW} + \gamma T_{SGD} + \delta T_{SMW}. \quad (2)$$

The set of all mixing equations can be written as the linear equation  $\mathbf{Ax} = \mathbf{b}$ , where matrix  $\mathbf{A} = [T; S; \dots]$  contains

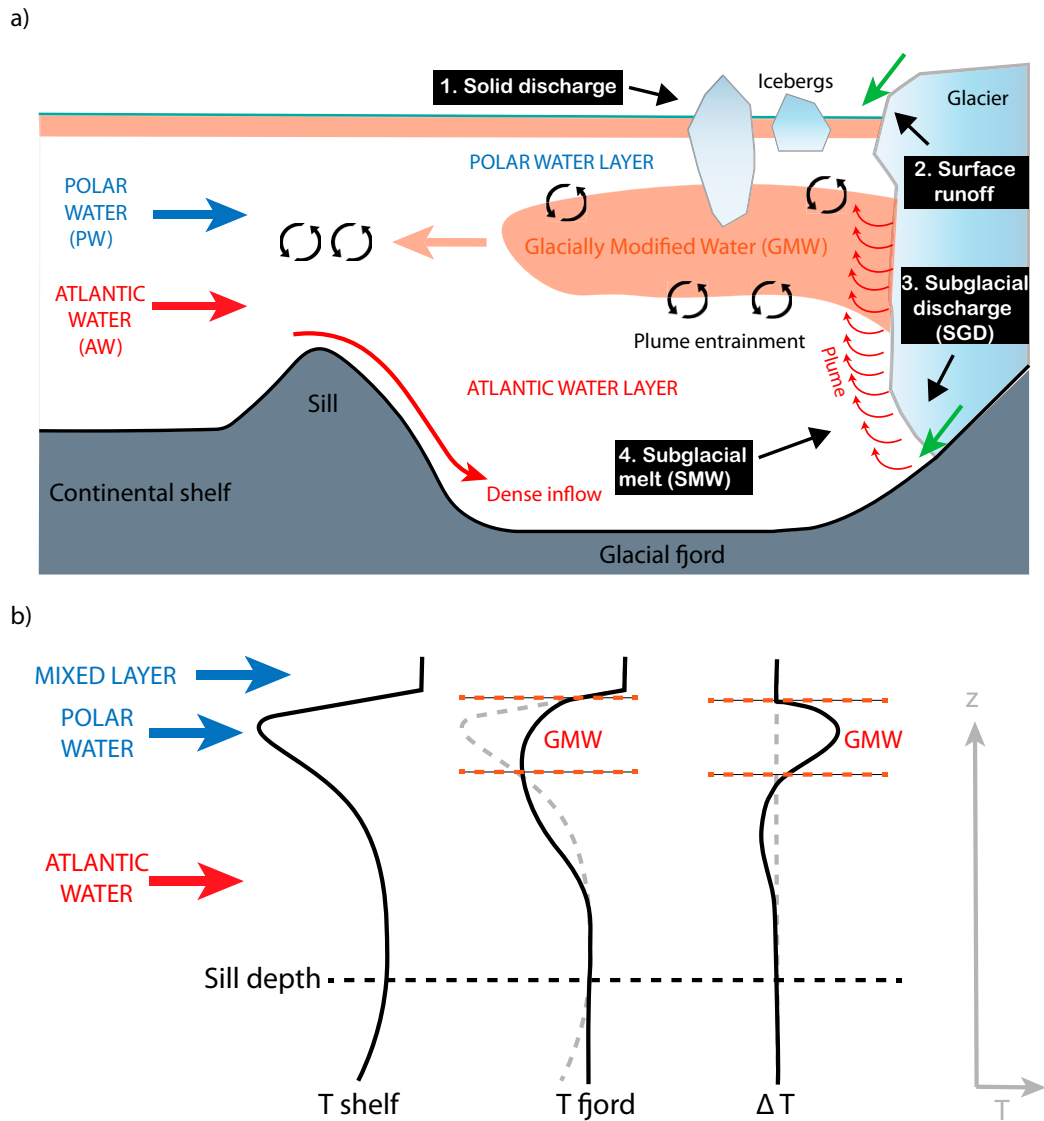


FIG. 3. (a) Schematic representation of the oceanic circulation in a typical Greenland glacial fjord with a marine-terminating glacier at its head (adapted from Straneo and Cenedese 2015). Black boxes indicate the four main sources of freshwater input to the fjord system which mix with the in-flowing Atlantic Water (AW) and Polar Water (PW) from the continental shelf, resulting in a buoyancy driven estuarine-type circulation and a diluted water mass mixture called Glacially Modified Water (GMW). Fjord and sill depths vary from fjord to fjord but typically range between 50 and 500 m and 100 and 1000 m, respectively (Sutherland et al. 2014). (b) Illustration describing how to define the GMW layer in the fjord using along-isopycnal temperature and salinity differences between the far field (shelf) and fjord. Farthest left we show the shape of a typical temperature profile on the shelf of northwest Greenland (e.g., Rysgaard et al. 2020), in the middle we show a typical shape of a temperature profile inside the fjord (e.g., Beaird et al. 2015; Straneo et al. 2011; Straneo et al. 2012), and farthest right we see the along-isopycnal difference between these two profiles. We define the GMW layer boundaries where the  $\Delta T$  profiles have positive anomalies. Typically, the isopycnal surfaces match geopotential surfaces very closely in the fjord, but we note that the anomalies are calculated in density coordinates.

all the variable values of the water masses contributing to the GMW (section 3b), vector  $\mathbf{b} = [T_{\text{GMW}} S_{\text{GMW}} \dots]$  gives the variable value of GMW and vector  $\mathbf{x} = [\alpha \beta \gamma \delta]$  gives the fractions that we are trying to solve for. We also

add the requirement that the sum of the fractions must equal one ( $\alpha + \beta + \gamma + \delta = 1$ ). Supposing we have  $n$  water masses and  $m$  measured water properties, then  $\mathbf{A}$  has dimensions  $m + 1 \times n$ . If  $m + 1 = n$  (i.e.,  $\mathbf{A}$  is a square

matrix), the solution of the linear system exists and is unique (if  $\mathbf{A}$  is nonsingular).

While [Beaird et al. \(2015\)](#) and [Beaird et al. \(2018\)](#) had access to noble gas concentrations, here we have only observed temperature and salinity ( $m = 2$ ). In our case, with  $n = 4$  water masses and given a single year/survey, this gives rise to an underdetermined system ( $m + 1 < n$ ). To make progress, we assume that water mass fractions are constant across multiple years and use the observed temperature and salinity from different years as independent parameters. We have two linear mixing equations for each year and with six years of observations, this results in  $m = 12$ , giving rise to an overdetermined system ( $m + 1 > n$ ). For an overdetermined system, the exact solution can be approximated in the least squares sense (e.g., [Björck 1996](#)), i.e., by minimizing the Euclidean norm of the residual  $\mathbf{r}$ , that is

$$\mathbf{x}^* \equiv \underset{\mathbf{x}}{\operatorname{argmin}} \|\mathbf{b} - \mathbf{A}\mathbf{x}\|_2 = \underset{\mathbf{x}}{\operatorname{argmin}} \|\mathbf{r}(\mathbf{x})\|_2. \quad (3)$$

We call our adaptation of the OMP method for optimum multi-parameter multiyear analysis (OMPM), and use a Monte Carlo method to provide an uncertainty estimate on this analysis ([Fig. A1](#)).

The constant fraction assumption is justifiable on the basis that the dominant parameters which influence the dilution are approximately constant in time. Specifically, dilution via entrainment in the plume is largely controlled by the depth at which the SGD is released (which can be assumed invariant barring major glacier retreat). Additionally, the dilution is controlled by the density difference between the fresh SGD water and the fjord waters (again largely constant since this difference is much greater than the interannual variations in density in the deep fjord waters) and also by the magnitude of the SGD [which does vary interannually but not sufficiently to substantially change the degree of meltwater dilution ([Fig. A2](#))]. The second dilution of the meltwaters is due to lateral mixing within the fjord, which is largely controlled by fjord geometry which, again, will not change sizably from one year to the next ([Carroll et al. 2017](#)). The validity of the assumption of constant fractions, furthermore, will be verified subsequently when we compute the residual in our analysis ([sections 4e](#) and [5c](#)).

*e. GMW from buoyant plume theory*

Buoyant plume theory from [Slater et al. \(2016\)](#) provides a complementary model for predicting the properties of GMW in the region close to the glacier front where one can assume that the GMW properties are largely controlled by the plume. Here we first assume an unstratified water column at the glacier front. The full plume model from [Slater et al. \(2016\)](#) can be run with a stratified water column as well, but then it can only be solved numerically. By simplifying the model input to one water mass only, we can solve the equations analytically. This approximation and the comparison to a stratified water column is further examined in [section 4e](#). In plume theory, the GMW properties are those of the buoyant upwelling plume once it reaches the surface

or a level of neutral buoyancy. Buoyant plume theory is based on classical plume geometry ([Morton et al. 1956](#)) and its application to marine-terminating glaciers by [Jenkins \(2011\)](#). Assuming that the GMW is a mixture of only AW, SGD, and SMW, its temperature and salinity are according to [Slater et al. \(2016\)](#) given by

$$T_{\text{GMW}} = \frac{Q_{\text{AW}}T_{\text{AW}} + Q_{\text{SGD}}T_{\text{SGD}} + Q_{\text{SMW}}T_{\text{SMW}}}{Q_{\text{AW}} + Q_{\text{SGD}} + Q_{\text{SMW}}}, \quad (4)$$

$$S_{\text{GMW}} = \frac{Q_{\text{AW}}S_{\text{AW}} + Q_{\text{SGD}}S_{\text{SGD}} + Q_{\text{SMW}}S_{\text{SMW}}}{Q_{\text{AW}} + Q_{\text{SGD}} + Q_{\text{SMW}}}, \quad (5)$$

where the  $Q$  represents the volume fluxes of each of the water masses. For a linear plume in an unstratified AW column with conservative temperature  $T_{\text{AW}}$ , absolute salinity  $S_{\text{AW}}$ , glacier grounding line depth  $h_{\text{gl}}$ , SGD  $Q_{\text{SGD}}$ , and channel width  $w$  (300 m), the entrained volume flux of the plume is ([Slater et al. 2016](#)):

$$Q_{\text{AW}} = \alpha h_{\text{gl}} \left( \frac{Q_{\text{SGD}} g'_0}{\alpha w} \right)^{1/3} w \quad (6)$$

where  $\alpha = 0.1$  is the entrainment coefficient and  $g'_0 = 0.26 \text{ m s}^{-2}$  is the reduced gravity of the plume at the grounding line, which in general depends on the temperature and salinity but can be taken to be roughly constant. Usually  $T_{\text{SGD}}$  is assumed to be the pressure melting point of freshwater at the glacier grounding line, given by  $T_{\text{SGD}} = \lambda_2 + \lambda_3 h_{\text{gl}}$  where  $\lambda_2 = 8.32 \times 10^{-2} \text{ }^\circ\text{C}$  and  $\lambda_3 = -7.53 \times 10^{-4} \text{ }^\circ\text{C m}^{-1}$  are constants for the freezing point offset and freezing point depth slope, respectively. [Slater et al. \(2016\)](#) also show that the SMW flux can be approximated as

$$Q_{\text{SMW}} = A_1 [1 + A_2 (T_{\text{AW}} - T_{\text{SGD}})] \left( \frac{Q_{\text{SGD}}}{w} \right)^{1/3} w h_{\text{gl}} \quad (7)$$

where  $A_1 = 1.56 \times 10^{-5} \text{ s}^{-2/3}$  and  $A_2 = 0.84 \text{ }^\circ\text{C}^{-1}$  are meltwater flux coefficients.

**4. Results**

*a. Upernavik fjord and shelf properties*

Here we present the first description of the water mass structure in Upernavik fjord from 2013 to 2019. In [Fig. 4](#), we show along-fjord hydrographic sections and accompanying shelf properties for four of the six years of observations in Upernavik (2013–19, excluding 2014). Surveys in 2017 and 2019 do not provide enough spatial coverage for a complete section. Temperature and salinity profiles for the shelf and fjord are shown in [Fig. 5](#). From 2013 to 2019, shelf profiles contain a thick layer of warm ( $1.7^\circ\text{--}2.9^\circ\text{C}$ ), salty ( $34.69\text{--}34.74 \text{ g kg}^{-1}$ ) AW, typically at depths below 300 m. The warmest AW core is at approximately 400 m, and below 500 m, the waters are slightly cooler. Overlying this AW layer is a colder ( $0^\circ\text{--}2^\circ\text{C}$ ) and fresher ( $33.8\text{--}34.6 \text{ g kg}^{-1}$ ), PW layer, with stratification rapidly increasing at the interface between these water masses. In general, isopycnals move upward from the

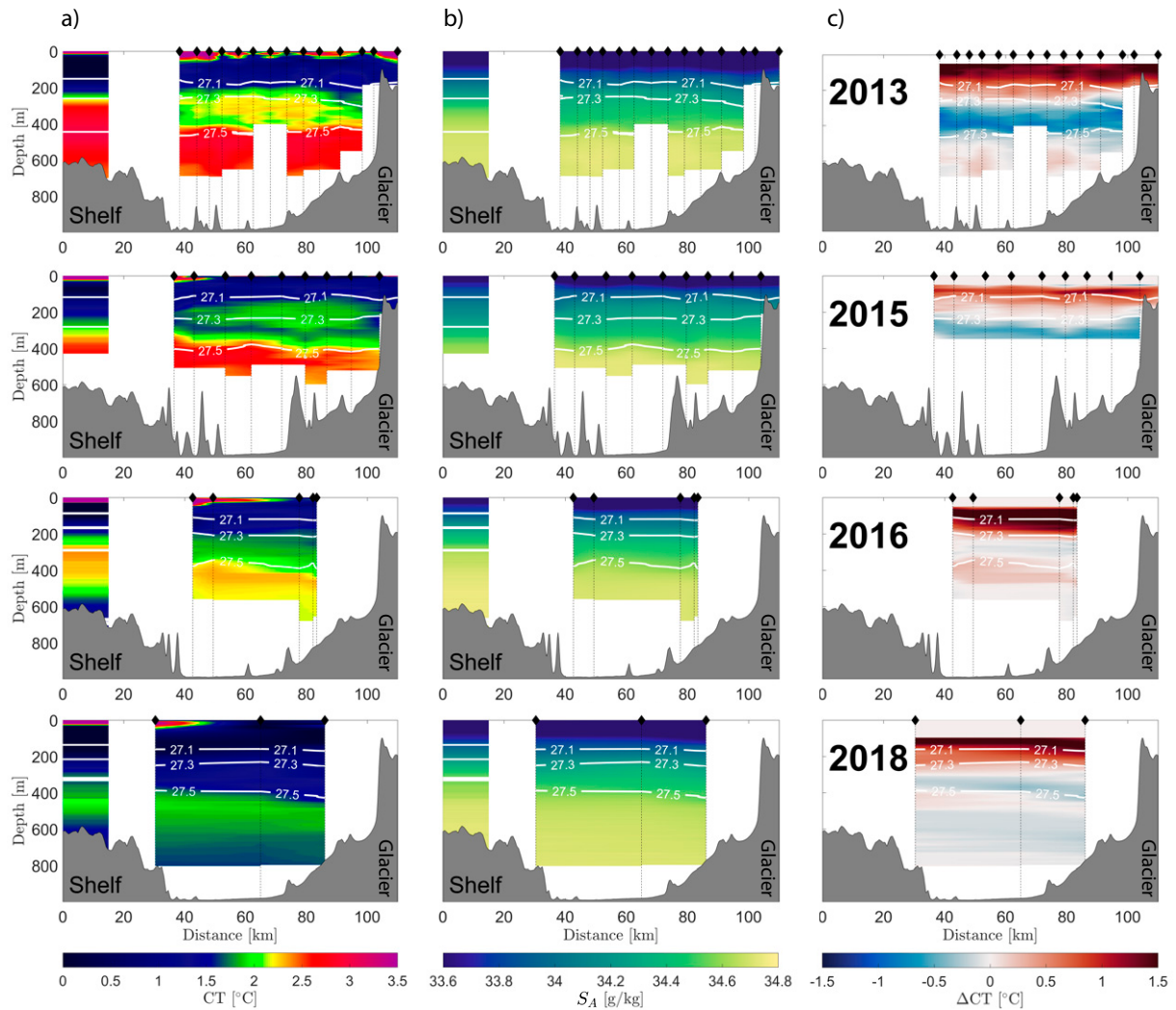


FIG. 4. Along-fjord (a) Conservative Temperature and (b) Absolute Salinity sections for 2013 (ship), 2015 (ship), 2016 (ship), and 2018 (OMG-AXCTD). Overlaid are three fixed density contours (white lines) and profile locations (dashed black lines). (c) The along-isopycnal temperature anomaly relative to the shelf. In these sections, the glacial fronts are located at distance approximately 120 km (right side of the figure) from the western starting point.

fjord to the shelf. At the surface (0–50 m), we typically find warmer and fresher waters. Since all profiles are taken during summer, the properties of this surface layer likely show influence from sea ice and iceberg melt, runoff from land, and solar warming. Generally, the water column structure remains relatively consistent between years (2013–19). However, there are significant variations in the temperature/salinity properties of all the water masses observed on the shelf (Table 2). The year-to-year variations are discussed in detail section 4c.

While the hydrographic structure is slightly more complex inside the fjord (Fig. 4), it follows the same general features of colder and fresher water masses overlying warm and salty AW, consistent also with that observed in other large glacial fjords in Greenland (Straneo et al. 2012). In contrast to the shelf surface waters, the fjord's surface waters are generally colder and fresher consistent with the discharge of cold

surface freshwater (e.g., from tundra melt and runoff). The along-fjord isopycnals are relatively flat from west to east, with a slight downward tilt toward the glacial fronts. Overall, there is limited spatial variability within the fjord, except for the upper layers in the stations closest to glacier fronts. This supports the notion that the mean fjord properties can still be captured in years with limited profiles within the fjord. Three across-fjord sections were collected in 2013 (one shown) and one in 2016. These support the assumption of limited across-fjord variability (Fig. 6). In the cross section closest to the glacier in 2013 and 2016, we see evidence of warmer AW being entrained above 400 m. In both 2013 and 2016, there is an across-fjord tilt in the dense  $27.5 \text{ kg m}^{-3}$  isopycnal, sloping down toward the northern side of the fjord, indicating a rotational effect. This suggests that the AW inflow into the fjord is more confined to the southern coast, as expected. In the



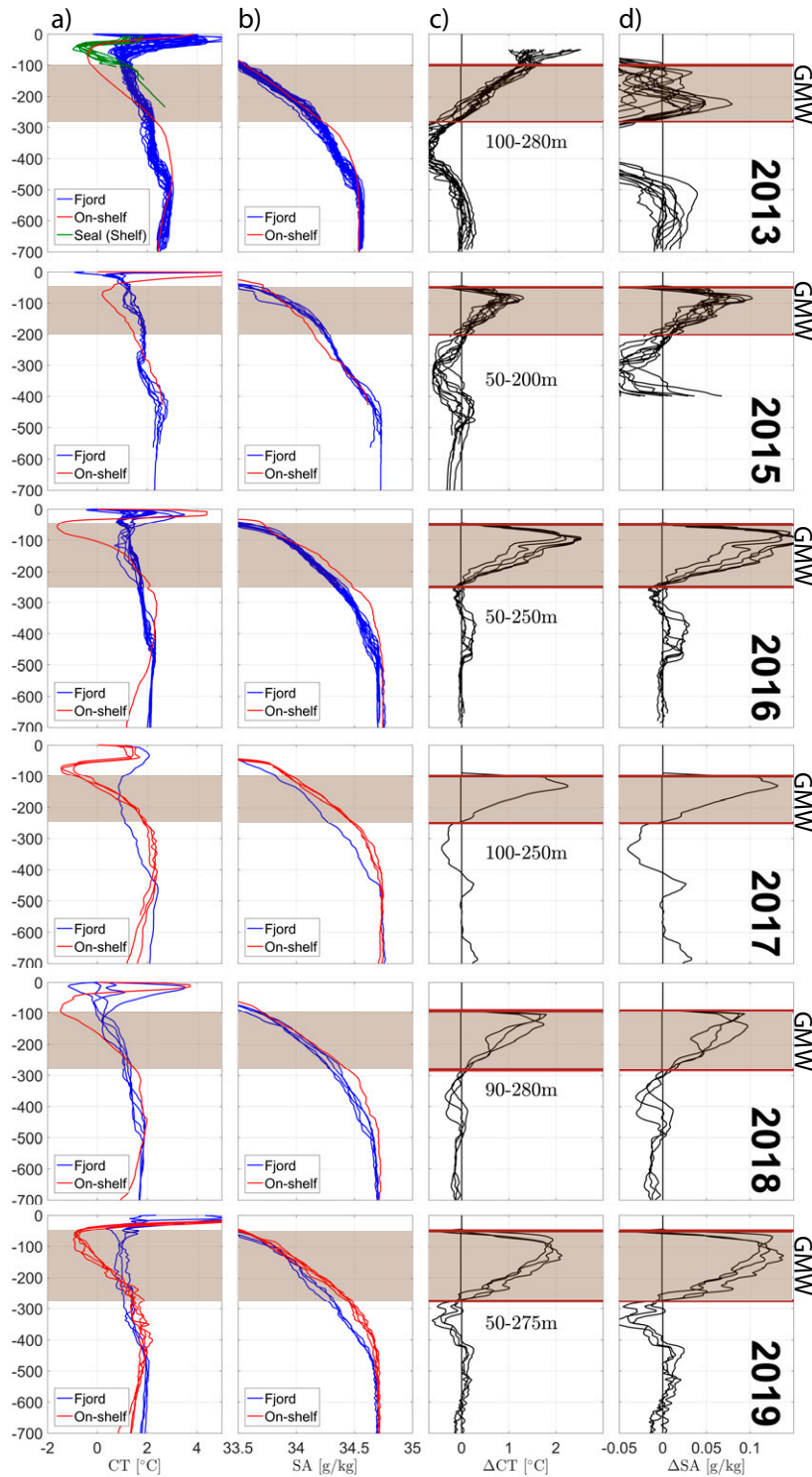


FIG. 5. Summer hydrographic profiles from the Upernavik fjord (blue) and shelf region (red) for 2013–19. (a) Conservative Temperature, (b) Absolute Salinity, (c)  $\Delta CT$ , (d)  $\Delta S_A$ . The upper and lower interfaces of the Glacially Modified Water layer (GMW) are indicated for each year by thick brown lines and light brown shading in (c) and (d) which correspond to the shading in density space in Fig. 7. Shallow green temperature profiles in 2013 are shelf profiles based on seal data. We note that  $\Delta CT$  and  $\Delta S_A$  are the along-isopycnal differences between the fjord and the shelf profiles and not the difference at the same depth coordinate.

TABLE 2. Fjord mean Conservative Temperature ( $^{\circ}\text{C}$ ) and Absolute Salinity ( $\text{g kg}^{-1}$ ) values of all observed water mass endmembers for each year. Uncertainty estimates used to perturb the design matrix in the Monte Carlo simulation for each water mass is given in the bottom row. AW is defined as the deep water mass in the fjord, which is unmodified from the shelf AW at sill depth. GMW is defined as the lighter water mass in the fjord, as described in section 3c. PW is defined as the light water mass on the shelf bounded by the same isopycnals as the GMW layer in the fjord.

	AW		PW		GMW	
	CT	$S_A$	CT	$S_A$	$\Theta$	$S_A$
2013	2.51	34.71	0.72	33.98	1.55	34.05
2015	2.36	34.72	0.98	34.00	1.51	34.01
2016	2.17	34.70	0.26	34.02	1.42	34.05
2017	2.21	34.74	-0.27	34.02	0.93	34.09
2018	1.70	34.69	-0.27	33.96	0.72	34.03
2019	1.79	34.69	-0.17	33.89	1.03	33.96
Uncertainty	0.1	0.05	0.1	0.05	—	—

westernmost section occupied in 2013 (not shown), the dense isopycnals ( $>27.5 \text{ kg m}^{-3}$ ) slope slightly downward toward the southern end. This could indicate potential wind-driven variability.

A comparison of the annual fjord and shelf profiles (Fig. 5) shows that, for the period 2013–19, the AW properties are usually identical at 450-m depth. Within the fjord, the AW properties below 450 m are entirely uniform, which is different from those present on the shelf. This might indicate the presence of a 450-m sill, between the fjord and the shelf, which limits the inflow into the fjord of waters below 450 m. However, the existence of such a sill is still to be confirmed since it is not present in the BedMachine V3 gridded product, which has a sill at the fjord's mouth at 600 m. Interannual variations in AW properties in the fjord match those on the shelf, supporting the idea that AW flows unmodified from the shelf into the fjord and is readily replenished on subannual time scales (Fig. 5). Annual mean fjord AW and shelf PW characteristics (following the definitions in section 3b) and their uncertainties for each year are presented in Table 2. From now on we treat the AW on the shelf (at 450 m) and in the fjord below 450 m as the same water mass, and neglect the AW on the shelf below this depth since it does not enter the fjord.

In summary, Figs. 4–6 and Table 2 provide the first description of the hydrographic structure in Upernavik. The structure (Fig. 5) and water mass properties (Table 2) vary moderately from year to year over the period 2013–19, but the AW is unmodified from the shelf to the fjord in all surveys. The properties of the upper layer differ between the fjord and the shelf, consistent with the expected transformation of waters inside the fjord by the glacier. Overall there is limited spatial variability in the fjord, except for cooling and freshening closest to the glacier fronts.

### b. GMW in Upernavik

Using the framework described in section 3b, we calculate the along-isopycnal temperature and salinity anomalies ( $\Delta\text{CT}$

and  $\Delta S_A$ ) for all fjord profiles relative to the shelf (Figs. 4 and 5). Based on these anomalies, we identify the lower and upper boundaries of the GMW layer for each year (Figs. 5 and 7). On average, we find that the GMW is approximately  $1\text{--}1.5^{\circ}\text{C}$  warmer and  $0.1 \text{ g kg}^{-1}$  saltier than the PW on the shelf, although this varies slightly from year to year (Table 2). We note that the differences are calculated based on the water masses bounded by the same isopycnals and not at the same depth coordinates (Fig. 7). In some year the difference between GMW and PW is small (e.g., in 2016), whereas in other years the difference is larger (e.g., in 2019). The difference is smallest when the PW and AW are warmer and saltier than the mean, and largest when the AW and PW are colder and fresher than the mean. In general, the GMW is about  $1.0^{\circ}\text{C}$  colder and  $0.7 \text{ g kg}^{-1}$  fresher than the AW.

The average thickness of the GMW layer is approximately 200 m, with year-to-year variations (Fig. 5). The temperature and salinity anomalies are largest at 50–200-m depth, suggesting that most of the upwelled water is found at these depths. Although the magnitude of the temperature and salinity anomalies vary from year to year, the overall anomaly distribution is constant over time. The temperature anomalies are largest in 2016, indicating that this could be a year with large differences between AW and PW characteristics on the shelf.

### c. GMW and AW variations 2013–19

Over the study period GMW temperatures have decreased, with a minimum in 2018 and a slight warming in 2019 (Fig. 8). Over the period 2013–18, the average GMW temperature decreased by  $0.8^{\circ}\text{C}$ . AW and PW temperatures have decreased over the same period, suggesting a close relationship between these water masses and GMW. Between 2013 and 2018, the maximum temperature in the AW observed within the fjord decreased by  $1.0^{\circ}\text{C}$ . Accompanying this cooling is a slight freshening of GMW ( $0.04 \text{ g kg}^{-1}$ ), AW ( $0.02 \text{ g kg}^{-1}$ ), and PW ( $0.04 \text{ g kg}^{-1}$ ). Although somewhat weaker, the cooling is consistent with the AW core temperature (200–250 m) upstream in Davis Strait (at  $67^{\circ}\text{N}$  and  $58^{\circ}\text{W}$ ) from the ECCO ocean state estimate (Fig. 8e), and temperature records from moorings in Disko Bay further south, where Khazendar et al. (2019) report cooling of  $1.5^{\circ}\text{C}$  in the AW layer between 2013 and 2018.

In the following two sections, we investigate the relationship between the AW, PW, and GMW in further detail, first by using an empirical model and second by using a buoyant plume model.

### d. GMW composition

Here we use the OMPM method described in section 3d to infer the composition of GMW. The fjord mean GMW, AW and PW temperature vary from year to year (Figs. 7 and 8). Solving the linear equations reveals that the GMW is made up of the following fractions:  $57.8\% \pm 8.1\%$  AW,  $41.0\% \pm 8.3\%$  PW,  $1.0\% \pm 0.1\%$  SGD, and  $0.2\% \pm 0.2\%$  SMW (Table 3, Fig. A1). The Monte Carlo tests (Fig. A1) indicate low sensitivity of the results to variations in the components in matrix **A**, supporting the constant fraction assumption.

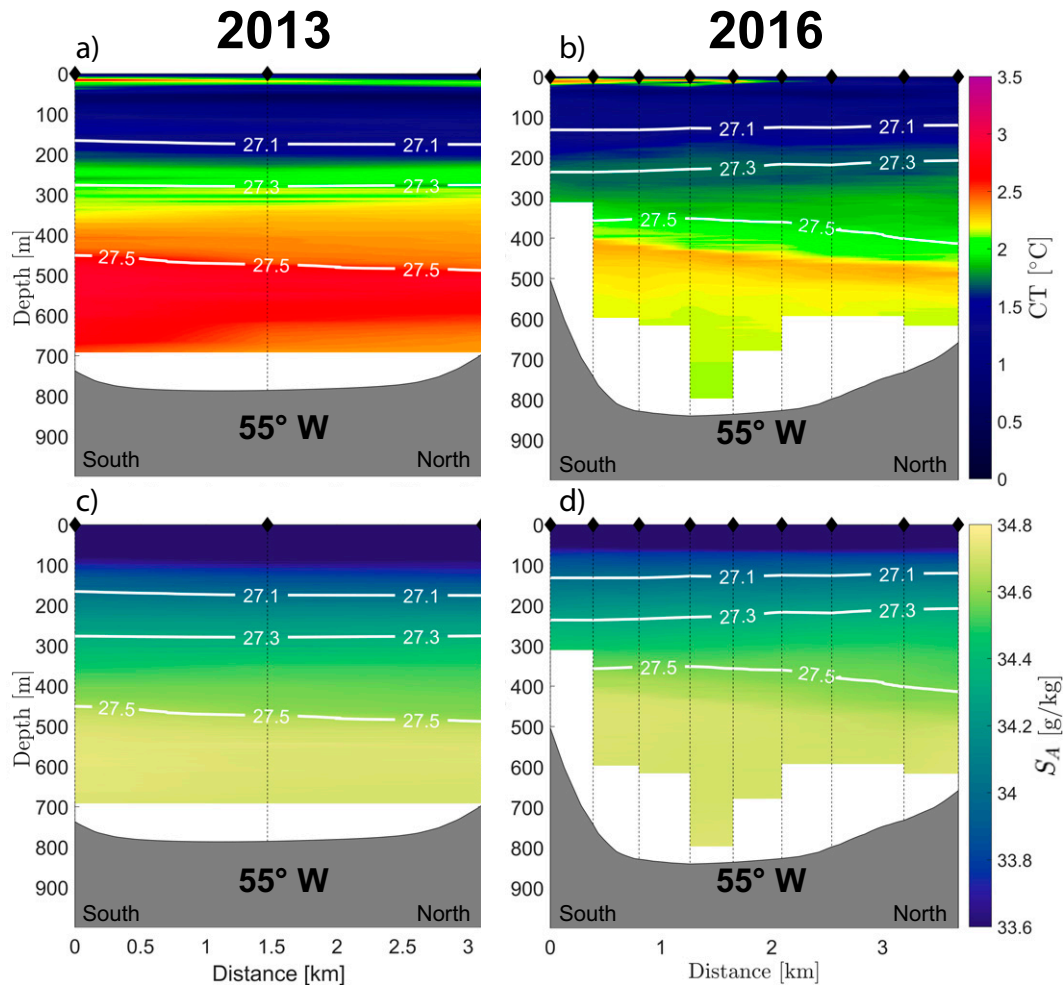


FIG. 6. Across-fjord (a),(b) Conservative Temperature and (c),(d) Absolute Salinity sections for 2013 (ship) and 2016 (ship). Overlaid are three fixed density contours (white lines) and profile locations (dashed black lines). See Fig. 2 for the section location.

Sensitivity tests also show that these results are not sensitive to excluding one or two years and not dominated by a specific year (not shown). It remains unclear exactly what determines the mixing fractions, but we hypothesize that the geometry of the fjord–glacier system plays an important role; comparison with other fjord–glacier systems would be helpful.

Using the OMPM-derived composition of GMW we can then re-estimate the properties of GMW in each year ( $GMW_{empir}$ ). By comparing to the observed properties of GMW in each year we can evaluate the success of the decomposition. The estimated and observed properties are close in every year (Fig. 7), validating the decomposition and supporting the assumption of constant fractional composition between years. Note that this exercise is essentially a restatement of the fact that the residual in the decomposition is small. Since the AW and PW make up most of the GMW mixture, it is logical to expect a close relationship between the AW, PW, and GMW variability. We next consider the extent to which buoyant plume theory is able to capture the properties of GMW.

*e. Reconstructing GMW properties using buoyant plume theory*

Plume theory provides a complementary means of estimating the properties of GMW from any single survey though we expect this to only hold within hundreds of meters of the glacier front (Mankoff et al. 2016). Further from the glacier front, we expect other processes, not accounted for by plume theory, to further modify the GMW as observed by De Andrés et al. (2020). Nonetheless, the buoyant plume theory provides a theoretical foundation for understanding the evolution of GMW.

Following the equations presented in section 3e, we calculate the properties of GMW according to buoyant plume theory for each year (Figs. 7 and 9a). Even though SGD volume varies seasonally and interannually (Fig. 9), our calculations assume a constant SGD of  $500 \text{ m}^3 \text{ s}^{-1}$  (the average for all five glaciers combined as simulated by RACMO, Fig. 9b) because the degree of mixing is not very sensitive to the SGD (Fig. A2). At first, we assume that AW is the only

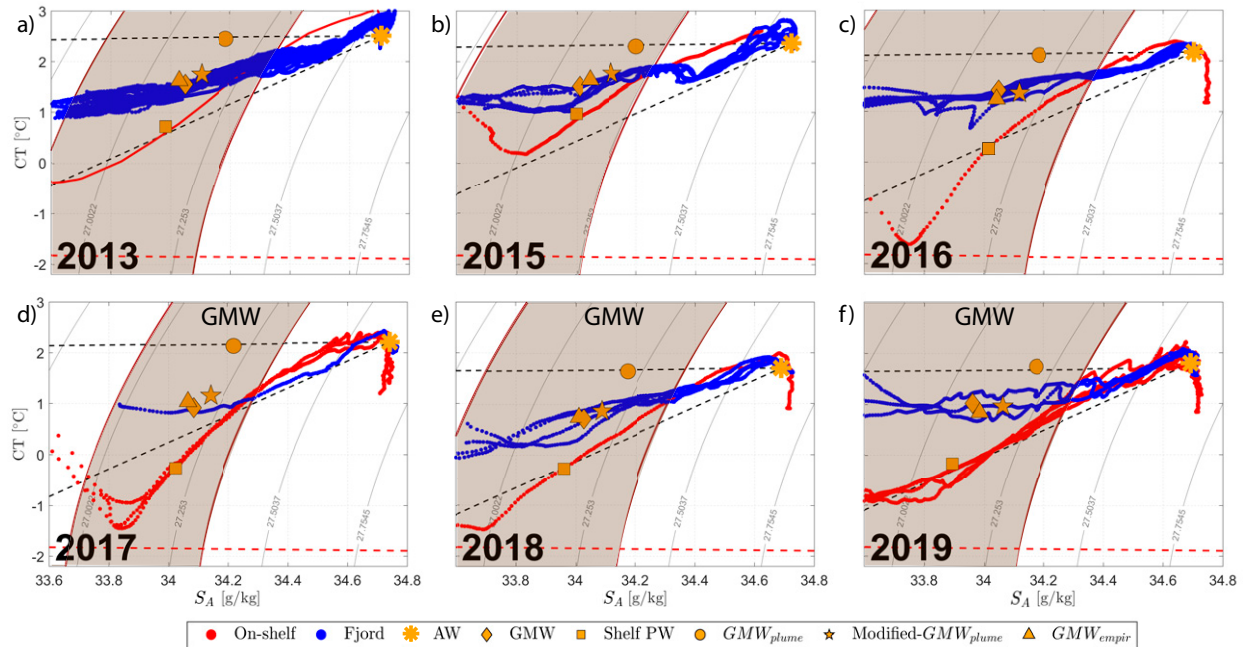


FIG. 7. Conservative Temperature and Absolute Salinity diagrams with all fjord (blue) and ambient shelf profiles (red) for the six years of hydrographic observations in Upernavik. The melting, runoff (black dashed) and freezing temperature (red dashed) lines are overlaid on all diagrams, along with fixed isopycnals (light gray). Brown shading indicates the isopycnal boundaries that define the GMW layer and correspond to brown lines in Fig. 5. Orange shapes indicate the average properties of AW, GMW, PW on the shelf,  $GMW_{plume}$ , Modified- $GMW_{plume}$ , and  $GMW_{empir}$ . Dashed lines indicate the runoff and melting mixing lines, which connect the ambient AW with SGD and SMW properties, respectively (see section 3c).

ambient water mass present at the glacier front (an unstratified water column). This has the advantage that we can then solve the plume model equations analytically. In reality, PW is also present at the glacier front. However, the presence of this PW does not significantly affect the properties of GMW because the majority of the mixing between the plume and ambient water occurs with AW. This can be seen by running the numerical plume model with the observed ambient fjord water masses as initial conditions and seeing that the results are very similar to running the model with AW only (Fig. A3). Significant differences are seen only above neutral buoyancy where the presence of PW cools the plume. Given our focus on neutral buoyancy in this study, it is therefore sufficient to consider a plume rising through unstratified AW.

The results ( $GMW_{plume}$ ) lie close to the runoff line in temperature/salinity space and are warmer and more saline than the observed GMW (Figs. 7 and 9a). This discrepancy is consistent with the notion that the plume theory neglects any mixing that occurs beyond the entrainment and upwelling associated with the plume. The average composition of the GMW predicted by the plume model,  $GMW_{plume}$ , is 98.8% AW, 1.16% SGD, and 0.04% SMW. If we add PW to the mixture until PW is 41% of the total [as suggested by the OMPM model (Table 3) and to reflect later mixing in the fjord], we get a water mass closer to the observed GMW (Fig. 7). We call this water mass *Modified- $GMW_{plume}$* . Modified-

$GMW_{plume}$  properties are closer to those of the GMW derived from the OMPM but are still too salty. This discrepancy could be explained by underestimating the flux of SGD from the glacier, overestimating the entrainment of AW into the plume, or neglecting some other source of freshwater. Nonetheless, this “modified plume theory” is in overall good agreement with the empirical mixing model proposed above. We note, however, that without the OMPM analysis we would not know how much PW should be added to the plume model results to derive the modified plume theory.

We can, on the other hand, use the plume model to investigate the sensitivity of  $GMW_{plume}$  properties to SGD volume, grounding line depth, and plume width (section b of the appendix). Overall the  $GMW_{plume}$  properties are not particularly sensitive to any of these quantities, except for  $GMW_{plume}$  salinity, which is slightly sensitive ( $\pm 0.8 \text{ g kg}^{-1}$ ) to variations in SGD volume ( $0\text{--}1000 \text{ m}^3 \text{ s}^{-1}$ ). It is, however, important to note that the SGD is critical in triggering the buoyant plume and hence the transformation associated with GMW formation.

#### f. Relationship between GMW, AW, and PW

By definition, in plume theory the properties of GMW would vary linearly with AW properties (section 3e). In reality, however, GMW properties vary with both AW and PW properties. Since the properties of SGD and SMW are

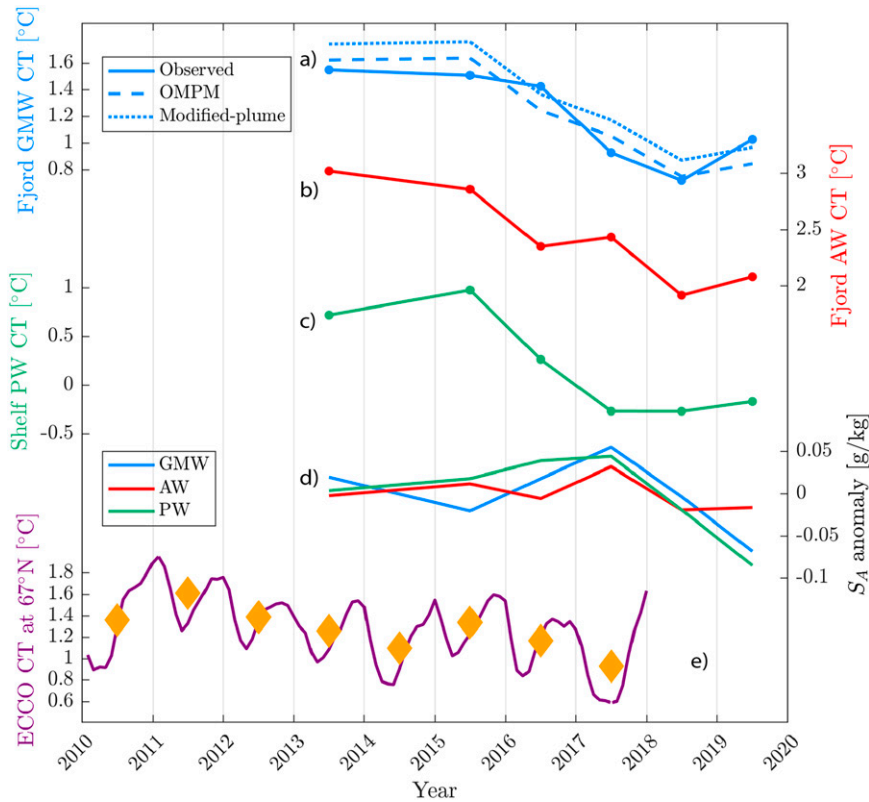


FIG. 8. Time series of Conservative Temperature for (a) GMW (blue), (b) AW (red), (c) PW (green), (d) Absolute Salinity (mean subtracted) in Upernavik fjord 2013–19, (e) upstream AW core temperature (200–250 m) in Davis strait (64°N) from the monthly mean ECCOV4 state estimate (purple line). Orange diamonds indicate the annual mean AW core temperature from ECCO to simplify comparison with (a)–(c).

constant (section 3c), and we assume constant fractional composition, we may write the expressions:

$$\Delta CT_{GMW} = \alpha \Delta CT_{AW} + \beta \Delta CT_{PW} \tag{8}$$

$$\Delta S_{A\_GMW} = \alpha \Delta S_{A\_AW} + \beta \Delta S_{A\_PW}, \tag{9}$$

where  $\alpha$  and  $\beta$  are the fractions derived in section 4d. Although GMW consists of roughly equal amounts of AW and PW, the GMW properties might still be more sensitive to one or the other because they vary with different amplitudes. Figure 10 shows the GMW properties as a function of both AW and PW. The variance explained by PW ( $R^2 =$

0.83 for temperature and  $R^2 = 0.75$  for salinity) is higher than by AW ( $R^2 = 0.69$  for temperature and  $R^2 = 0.40$  for salinity), even though AW makes up a larger fraction of the GMW composition. This indicates that the GMW properties could be more sensitive to changes in PW than in AW, although the slope of the AW curve shows that a change in AW has a larger effect than a change in PW. Here we note that there are only six data points and that these relationships are not statistically significant. Also, both the data and our understanding of the circulation around Greenland suggests that PW is likely not completely independent from AW (since PW reaching the Upernavik system is likely to have already been mixed with some AW as it flows around Greenland), and we therefore suggest that AW and PW contribute at roughly equal weight.

## 5. Discussion

### a. Upernavik as a case study for Greenland fjords

We now ask the question to what extent do our results apply to other glacier–fjord systems in Greenland. This is particularly important if we want to derive fractional compositions and exchange fluxes as inputs to large-scale ocean

TABLE 3. Water mass composition fractions that make up GMW composition in Upernavik. The values correspond to the constants ( $\alpha$ ,  $\beta$ ,  $\gamma$ , and  $\delta$ ) in Eq. (2). The uncertainty is calculated based on the Monte Carlo analysis as described in the appendix.

AW (%)	PW (%)	SGD (%)	SMW (%)
$0.8 \pm 8.1$	$41.0 \pm 8.3$	$1.0 \pm 0.1$	$0.2 \pm 0.2$

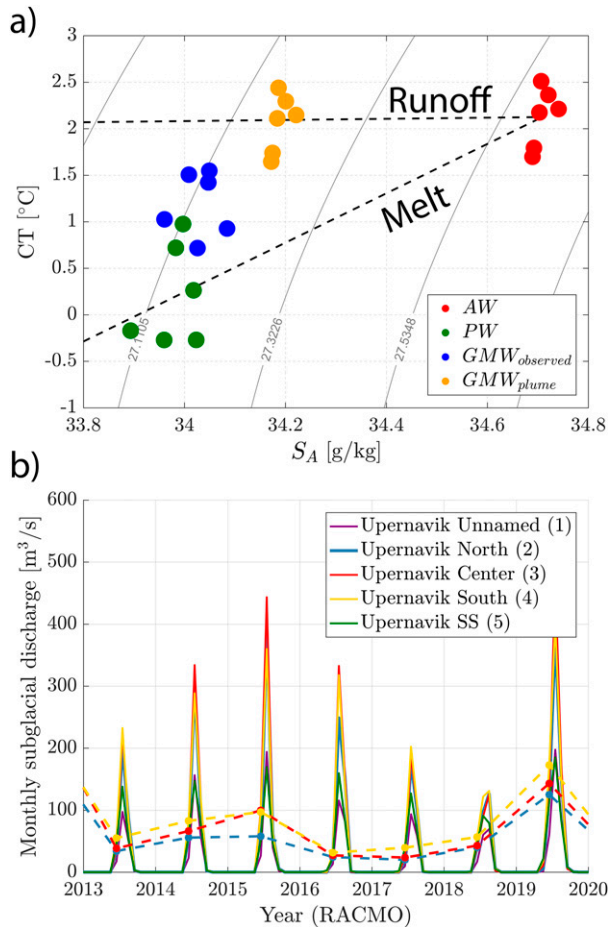


FIG. 9. Conservative Temperature and Absolute Salinity diagram with all mean water masses properties 2013–19. Warm and saline AW (red circles) is mixed with colder and fresher PW (green dots), SGD and SMW to produce a mixture of GMW (blue dots). (b) Monthly mean time series of simulated SGD from RACMO for all marine-terminating glaciers in Upernavik as indicated in Fig. 2. Dashed lines represent the mean August runoff for the three largest glaciers.

models. We speculate that that our method could be applied to any fjord with a two layer structure since we expect that the GMW will mix with a lighter layer after having upwelled past the layer interface. We base our speculation on the fact that the hydrographic properties and circulation of five glacier–fjord systems along Greenland’s coast (79 North, Kangerlussuaq, Helheim, Petermann and Jacobshavn) have similar structures (Straneo et al. 2012). In particular AW at grounding-line depth and SGD apply to all these glaciers. Although the hydrographic properties in these fjords depend on the shelf bathymetry (i.e., presence of canyons) and sill depth, the overall structure is very similar to that of Upernavik. The fjord profiles studied by Straneo et al. (2012) also show that properties are usually similar to the shelf profiles at depth (with the exception of Jacobshavn, which has a shallow sill). Strong stratification persists in the fjords, but unlike the

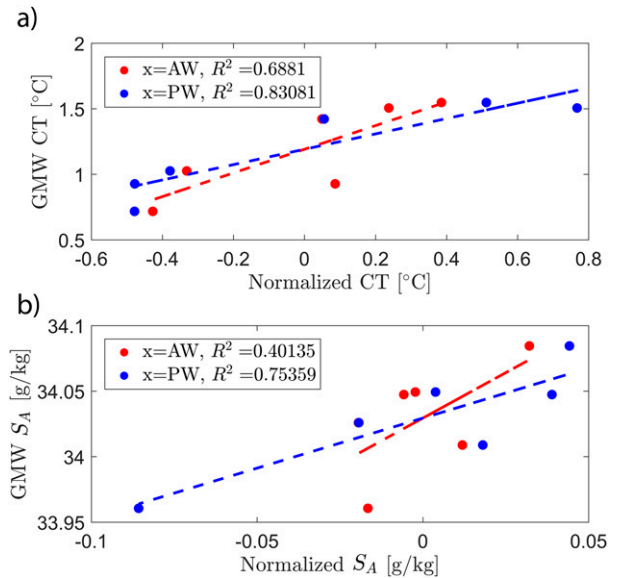


FIG. 10. GMW temperature as a function of AW<sub>obs</sub> temperature (red dots) and PW (blue dots) temperature. Dashed lines represent a linear fit based on the six years of observations. Mean values of AW<sub>obs</sub> and PW have been subtracted to visualize the data on a comparable scale. (b) As in (a), but for salinity.

AW, the layer with density comparable to the PW layer has been strongly modified in all fjords (Straneo et al. 2012), similar to what we observe in Upernavik. In the upper part of the water column, fjord waters are generally warmer than the shelf waters, indicating modified AW upwelling at the glacier fronts and in the ice melange. There is a “runoff” point in most fjord systems, where the *T/S* characteristics within the fjord veer from the melting toward the runoff line. We observe this in Upernavik as well, and this point coincides with the lower boundary of our GMW layer. Similar hydrographic characteristics were reported by Johnson et al. (2011) and Heuzé et al. (2016) for Petermann fjord, Inall et al. (2014) for Kangerlussuaq fjord, and Sutherland et al. (2014) for Sermilik and Kangerlussuaq fjords. Fjords with a very shallow sill, such as Jacobshavn and Godthåbsfjord (Mortensen et al. 2011) are likely to have slightly different hydrography.

The similarity in hydrography between Upernavik and these other fjord systems indicates that the method utilize to identify GMW and to derive its fractional composition, given multiple surveys, could potentially work for other fjord systems. We expect, however, that the fractional composition of the GMW will vary from one fjord system to the next since it is likely set by factors such as fjord geometry (such as the presence of sills), spatial scales, grounding line depth and the magnitude of SGD.

#### b. Prospects for parameterizing fjord to shelf exchange

We show that the exported GMW properties may be expressed as a function of the combined AW and PW on the continental shelf. This simple relationship could be used to

form a parameterization for large-scale ocean models that do not resolve the fjords or glacier/ocean interactions (Böning et al. 2016; Dukhovskoy et al. 2019). A better representation of GMW in models is needed to properly understand the effect of freshwater on the ocean. An ideal parameterization or the exchange of heat, freshwater, and mass at the margins of Greenland's fjords will take as inputs oceanic conditions on the continental shelf (e.g., AW and PW), geometric constraints (e.g., sills), glacier characteristics and glacial inputs (SGD) and yield melt rates, the volume fluxes, and properties of both the outflow and inflow at the fjord's mouth. Our results indicate that repeat surveys can be used to derive the fractional composition of GMW, that its fractional composition can be assumed invariant, and that once we know this, we can determine the relative roles of PW and AW in the variability of GMW. Future work is needed to establish what sets these fractions in each fjord system and whether they could be determined a priori from a knowledge of the external parameters of the fjord and glacier without observations to inform their values.

An ideal "glacier-forcing" parameterization (or submodel) for ocean models would include not just the exchange properties but also an estimate of the exchange flow, i.e., the volume transport of the diluted meltwater (GMW) which is compensated by the inflow of shelf water into the fjord. The exchange flow is not equal to the glacial input but, similar as in estuarine literature (i.e., MacCready and Geyer 2010), equal to transport out of the fjord in the upper layers which is largely balanced by the transport in the lower layers. While measurements from Upernavik did not allow for an estimate of the volume exchange from data, we can use the mixing model to provide a first assessment of this exchange. Given the constant fractional composition assumption and knowledge that SGD makes up  $1.0\% \pm 0.1\%$  of the GMW, an average summer SGD of  $500 \text{ m}^3 \text{ s}^{-1}$  then translates into an exchange flux of  $50 \pm 5 \text{ m Sv}$  GMW (excluding the surface layer). Given the dimensions of the fjord and thickness of the GMW layer, this would be achieved by an outflow of  $3 \text{ cm s}^{-1}$ , comparable to  $5 \text{ cm s}^{-1}$  found in quantifying the mean summertime exchange flow in Sermilik fjord by Beaird et al. (2018). The implication is that if we know the fractional composition for a fjord system, and can estimate the input of SGD (which is less uncertain than derivations of the iceberg and submarine melt), then one can estimate the GMW export even without current observations. More work is needed to determine to what extent this method can be generalized to other systems in Greenland and the extent to which this flux derivation is valid.

In the same way as ocean models need parameterizations to represent the ice sheet's freshwater forcing on the ocean, ice sheet and glacier models need parameterizations of oceanic forcing (Slater et al. 2016; Morlighem et al. 2019). Due to a lack of observations and time series from within the fjords, oceanic thermal forcing and melt rates for ice sheet and regional glacier models are currently mainly based on hydrographic observations from the shelf (Wood et al. 2021).

In these cases, the AW properties and variability are extrapolated from the shelf into the fjords at sill depth. The study in Upernavik confirms that changes in AW property on the shelf result in identical changes in AW property in the fjords above sill depth. However, accurate bathymetry is necessary, as an error in sill depth would result in large differences in simulated fjord water mass properties and melt rates. Given the hydrographic similarities with other fjords, it is reasonable to assume that this holds for other fjords with a deep enough connection to the shelf.

### c. Limitations of this study

Our analysis does not allow to distinguish between iceberg melting in the fjords (Moon et al. 2018) and submarine melting, as such, it cannot provide an estimate of submarine melting to be used to force glacier and ice sheet models. We also neglect the surface layer, where a significant part of the export of freshwater occurs (Beaird et al. 2018). This is because of the larger degree of variability of properties in this upper layer and the fact that because of air-sea exchanges and sea ice melt we cannot assume that properties in this layer are due to glacier/ocean interaction alone. Still, much of the GMW associated with upwelling driven by SGD should be represented in our proposed formulation. Atmospheric conditions are important for the renewal of fjord waters (e.g., Christoffersen et al. 2011; Jackson et al. 2014; Jackson et al. 2018), but due to limited atmospheric observations we did not have the possibility to properly investigate the role of atmospheric forcing on GMW export.

Besides comparing the AW variations observed on the Upernavik shelf to upstream AW variations in Davis Strait (section 4c), we do not investigate the mechanisms causing variations in AW and PW. However, we note that the AW variability is likely advective (Cuny et al. 2005; Sutherland and Pickart 2008) and that PW variability is likely not completely independent from AW. The PW often resides on the meltwater-mixing line from that year's AW properties (Fig. 7), indicating that the PW outside Upernavik may contain meltwater from upstream.

A limitation of our method used to identify GMW is that it is dependent on comparing shelf and fjord properties. This requires having both sets of profiles and, also, assuming that the properties at the shelf profile location do not contain GMW exported from the fjord. Moreover, we started out with an assumption that the fractional composition remains constant in time, which our results suggest works for Upernavik. While further work is required to test the applicability of this assumption to other fjords, we believe it is quite likely to hold given the dominant role of fjord-glacier geometry in controlling the mixing processes, and the fact that interannual variations in density within the fjord are small compared to the density difference between SGD and the other water masses. Additionally, buoyant plume theory indicates that GMW properties are only moderately sensitive to changes in SGD.

Finally, we note that there are other ways of calculating glacial meltwater concentration, such as for example done in

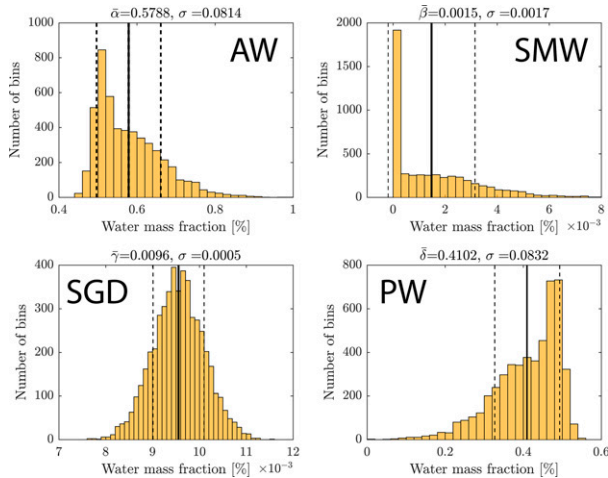


FIG. A1. Error distribution for the water mass fractions making up the GMW mixture resulting from a Monte Carlo simulation with 5000 iterations. Mean values for the various water mass fractions are represented by thick black lines, and their uncertainty is given by one standard deviation (dashed black lines).

the Petermann Fjord by Heuzé et al. (2016) which provides an alternative method to determine the depth of GMW export.

## 6. Conclusions

Upernavik is a fjord in northwest Greenland that receives a large (seasonal) freshwater contribution from surface melting [as subglacial discharge (SGD) and runoff from land], solid ice flux (calving icebergs), and Submarine Melt Water (SMW). We here present the first description of water mass characteristics in Upernavik fjord from summer hydrographic observations over six years between 2013 and 2019. Dense Atlantic Water (AW) and lighter Polar Water (PW) found in Upernavik fjord and on the Upernavik shelf has gradually cooled ( $1.0^{\circ}\text{C}$ ) and freshened ( $0.02 \text{ g kg}^{-1}$ ) throughout 2013–19, consistent with AW cooling observed further upstream (south) in Disko Bay and Davis Strait (Khazendar et al. 2019). By comparing anomalies on the shelf and in the fjord, and building on our understanding of the dynamics of glacial fjords, we have derived the properties of the main water mass exported from the fjord: Glacially Modified Water (GMW). The depth of GMW varies from year to year, with a typical range of approximately 50–200 m. Using a water mass analysis method called optimum multi-parameter multiyear analysis we estimate that GMW is composed of approximately 58% AW, 41% PW, 1% SGD, and 0.2% SMW. These fractions are similar to those derived from studies based on noble gases from other fjord systems in Greenland (Beaird et al. 2015, 2018), and from this follows a rough estimate of a total (summer) GMW export of approximately 50 mSv. The change in GMW properties observed is consistent with the changes in AW and PW on the shelf, in that GMW variability can be expressed as a linear function of the combined AW

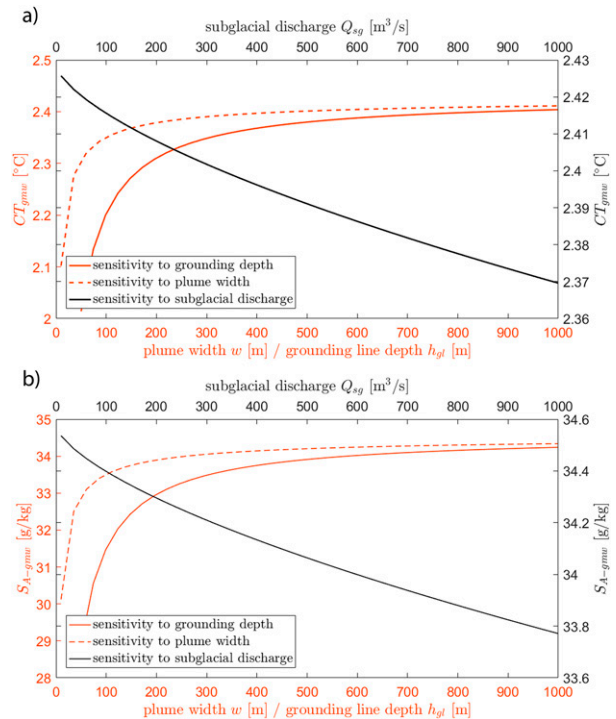


FIG. A2. Sensitivity of Upernavik GMW (a) temperature and (b) salinity on changes in grounding depth, plume width and SGD based on plume theory (Slater et al. 2016). Orange lines represent the sensitivity to changes in grounding depth (whole lines) and plume width (dashed lines) as represented by the lower x axis. Black lines represent the sensitivity to changes in SGD (top x axis and rightmost y axis).

and PW variability. Comparison with a buoyant plume model shows that the model alone cannot accurately reproduce GMW properties. Consistent with other studies, we believe this is due to the fact that the plume model does not account for further mixing that occurs after the plume has reached neutral buoyancy. This study provides the first basis for the development of a parameterization for the export of GMW from glacial fjords in coarse resolution models, however, further work is required to test the transferability of the conclusions across Greenland's diverse glacial fjords.

**Acknowledgments.** This work was partially supported by the Centre for Climate Dynamics (SKD) at the Bjerknes Centre for Climate Research. The authors thank NASA and the OMG consortium for making observational data freely available, and acknowledge M. Morlighem for good support in the early stages of this project. MM and LHS would also like to thank Ø. Paasche, the ACER project, and the U.S. Norway Fulbright Foundation for the Norwegian Arctic Chair Grant 2019–20 that made the visit to Scripps Institution of Oceanography possible. FS acknowledges support from the DOE Office of Science Grant DE-SC0020073, Heising-Simons Foundation and from NSF and OCE-1756272. DAS acknowledges support from U.K. NERC Grants NE/P011365/1, NE/T011920/1, and



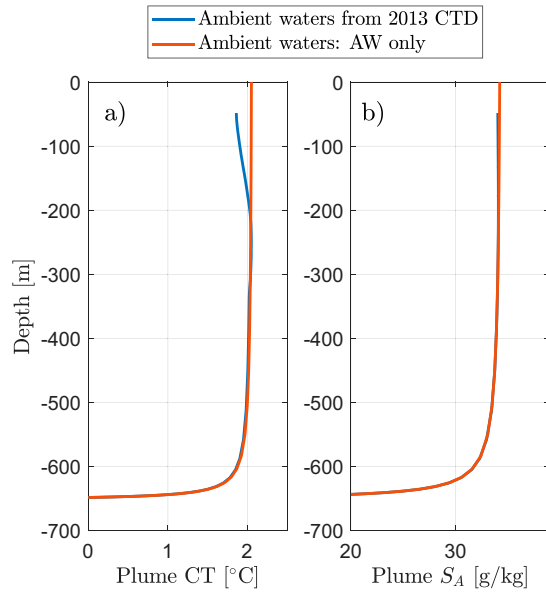


FIG. A3. Profiles of (a) plume temperature and (b) plume salinity from the buoyant plume model (Slater et al. 2016). Modeled properties when forcing the model with ambient waters according to a 2013 CTD are shown in blue (mostly hidden beneath orange), and modeled properties when forcing with unstratified AW are shown in orange.

NERC Independent Research Fellowship NE/T011920/1. MW was supported by an appointment to the NASA Postdoctoral Program at the Jet Propulsion Laboratory, California Institute of Technology, administered by the Universities Space Research Association under contract with NASA. CSA would like to acknowledge Geocenter Denmark for support to the project “Upernavik Glacier.” We gratefully acknowledge the many scientists, engineers, and mariners who went to sea to collect the observational data, without whom this study would not be possible.

*Data availability statement.* The full Upernavik CTD data-set used in this study (2013–19) is publicly available at the online Arctic Data Center repository: doi:10.18739/A2SJ19S1Q. OMG CTD data are also available at the OMG website: <https://omg.jpl.nasa.gov/portal/browse/>. The ECCO Version 4 Release 3 and Version 5 Release alpha ocean and sea-ice products are available at <http://ecco.jpl.nasa.gov> and <ftp://ecco.jpl.nasa.gov/Version5/Alpha/>. Bed topography and fjord bathymetry Bed-Machine Version v3 data are available at <http://sites.uci.edu/morlighem/dataproducts/bedmachine-greenland>.

APPENDIX

Uncertainty and Sensitivity

a. Uncertainty in the fractional composition of GMW

The uncertainty in the solution for the water mass fractions given by vector  $\mathbf{x}$  in Eq. (6) is evaluated using a Monte Carlo method following Beaird et al. (2018). The

TABLE A1. GMW properties (mean and standard deviation over 6 years) based on various definitions of GMW. The top row is the definition used in this paper and is the only definition that captures the whole GMW layer each year. The second row is the same but has the surface layer (uppermost 50 m) included as well. Fixed depth definitions (row 5–10) do not capture the whole GMW layer, as the depth varies from year to year.

GMW definition	CT (GMW) (°C)		$S_A$ (GMW) (g kg <sup>-1</sup> )	
	Mean	Std dev	Mean	Std dev
50 m— $\Delta CT$ and $\Delta S_A \geq 0$	1.191	0.317	34.03	0.04
0 m— $\Delta CT$ and $\Delta S_A \geq 0$	1.252	0.298	33.77	0.10
max( $\Delta CT$ ) $\pm 50$ m	1.083	0.298	33.94	0.04
max( $\Delta CT$ ) $\pm 100$ m	0.993	0.302	33.84	0.05
50–250 m	1.174	0.337	33.95	0.09
50–150 m	1.045	0.354	33.75	0.12
100–150 m	1.011	0.375	33.91	0.10
100–200 m	1.103	0.379	33.99	0.09
100–250 m	1.205	0.371	34.07	0.08
0–250 m	1.248	0.320	33.75	0.15

5000 perturbed versions of the matrix  $\mathbf{A}$  and Eq. (6) are created where all the elements in  $\mathbf{A}$  are replaced by perturbed water mass values selected from a random normal distribution with mean values from the original matrix  $\mathbf{A}$  and standard deviation given by the uncertainty estimates ( $\epsilon$ , Table 2) for each parameter in  $\mathbf{A}$ . The standard deviation of these 5000 solutions (Fig. A1) represents the systematic uncertainty in the water mass fractions in Table 3. Table A1 shows the average properties of GMW based on different definitions, as discussed in section 3b.

b. Sensitivity of GMW properties from plume theory

Figure A2 shows results of a sensitivity test using the plume model. For shallow grounding-line depths (<200 m) the GMW temperature and salinity are quite sensitive to changes in grounding-line depth ( $\pm 0.4^\circ\text{C}$  and  $\pm 5 \text{ g kg}^{-1}$ , respectively). For grounding-line depths deeper than 200 m the GMW properties are not sensitive to changes in grounding-line depth. Similarly, for wide plumes (>50 m) the GMW properties are not sensitive to changes in plume width. The GMW temperature is not very sensitive to changes in SGD volume ( $\pm 0.05^\circ\text{C}$ ). The GMW salinity, on the other hand, is more sensitive to the volume of SGD driving the plume ( $\pm 0.8 \text{ g kg}^{-1}$ ).

REFERENCES

Andresen, C. S., K. K. Kjeldsen, B. Harden, N. Nørgaard-Pedersen, and K. H. Kjær, 2014: Outlet glacier dynamics and bathymetry at Upernavik Isstrøm and Upernavik Isfjord, North-West Greenland. *GEUS Bull.*, **31**, 79–82, <https://doi.org/10.34194/geusb.v31.4668>.  
 Bamber, J., M. van den Broeke, J. Ettema, J. Lenaerts, and E. Rignot, 2012: Recent large increases in freshwater fluxes

- from Greenland into the North Atlantic. *Geophys. Res. Lett.*, **39**, L19501, <https://doi.org/10.1029/2012GL052552>.
- Bamber, J. L., A. J. Tedstone, M. D. King, I. M. Howat, E. M. Enderlin, M. R. van den Broeke, and B. Noel, 2018: Land ice freshwater budget of the Arctic and North Atlantic Oceans: 1. Data, methods, and results. *J. Geophys. Res. Oceans*, **123**, 1827–1837, <https://doi.org/10.1002/2017JC013605>.
- Beaird, N., F. Straneo, and W. Jenkins, 2015: Spreading of Greenland meltwaters in the ocean revealed by noble gases. *Geophys. Res. Lett.*, **42**, 7705–7713, <https://doi.org/10.1002/2015GL065003>.
- , —, and —, 2017: Characteristics of meltwater export from Jakobshavn Isbræ and Ilulissat Icefjord. *Ann. Glaciol.*, **58**, 107–117, <https://doi.org/10.1017/aog.2017.19>.
- Beaird, N. L., F. Straneo, and W. Jenkins, 2018: Export of strongly diluted Greenland meltwater from a major glacial fjord. *Geophys. Res. Lett.*, **45**, 4163–4170, <https://doi.org/10.1029/2018GL077000>.
- Björck, Å., 1996: *Numerical Methods for Least Squares Problems*. SIAM, 407 pp.
- Björck, A. A., L. M. Kruse, and P. B. Michaelsen, 2015: Brief communication: Getting Greenland's glaciers right—a new data set of all official Greenlandic glacier names. *Cryosphere*, **9**, 2215–2218, <https://doi.org/10.5194/tc-9-2215-2015>.
- Böning, C. W., E. Behrens, A. Biastoch, K. Getzlaff, and J. L. Bamber, 2016: Emerging impact of Greenland meltwater on deepwater formation in the North Atlantic Ocean. *Nat. Geosci.*, **9**, 523–527, <https://doi.org/10.1038/ngeo2740>.
- Caesar, L., G. D. McCarthy, D. J. R. Thornalley, N. Cahill, and S. Rahmstorf, 2021: Current Atlantic Meridional Overturning Circulation weakest in last millennium. *Nat. Geosci.*, **14**, 118–120, <https://doi.org/10.1038/s41561-021-00699-z>.
- Carroll, D., D. A. Sutherland, E. L. Shroyer, J. D. Nash, G. A. Catania, and L. A. Stearns, 2015: Modeling turbulent subglacial meltwater plumes: Implications for fjord-scale buoyancy-driven circulation. *J. Phys. Oceanogr.*, **45**, 2169–2185, <https://doi.org/10.1175/JPO-D-15-0033.1>.
- , —, —, —, —, and —, 2017: Subglacial discharge-driven renewal of tidewater glacier fjords. *J. Geophys. Res. Oceans*, **122**, 6611–6629, <https://doi.org/10.1002/2017JC012962>.
- , and Coauthors, 2018: Subannual and seasonal variability of Atlantic-origin waters in two adjacent west Greenland fjords. *J. Geophys. Res. Oceans*, **123**, 6670–6687, <https://doi.org/10.1029/2018JC014278>.
- Christoffersen, P., R. I. Mugford, K. J. Heywood, I. Joughin, J. A. Dowdeswell, J. P. M. Syvitski, A. Luckman, and T. J. Benham, 2011: Warming of waters in an East Greenland fjord prior to glacier retreat: Mechanisms and connection to large-scale atmospheric conditions. *Cryosphere*, **5**, 701–714, <https://doi.org/10.5194/tc-5-701-2011>.
- Cuny, J., P. B. Rhines, and R. Kwok, 2005: Davis Strait volume, freshwater and heat fluxes. *Deep-Sea Res. I*, **52**, 519–542, <https://doi.org/10.1016/j.dsr.2004.10.006>.
- Curry, B., C. M. Lee, and B. Petrie, 2011: Volume, freshwater, and heat fluxes through Davis Strait, 2004–05. *J. Phys. Oceanogr.*, **41**, 429–436, <https://doi.org/10.1175/2010JPO4536.1>.
- , —, —, R. E. Moritz, and R. Kwok, 2014: Multiyear volume, liquid freshwater, and sea ice transports through Davis Strait, 2004–10. *J. Phys. Oceanogr.*, **44**, 1244–1266, <https://doi.org/10.1175/JPO-D-13-0177.1>.
- De Andrés, E., D. A. Slater, F. Straneo, J. Otero, S. Das, and F. Navarro, 2020: Surface emergence of glacial plumes determined by fjord stratification. *Cryosphere*, **14**, 1951–1969, <https://doi.org/10.5194/tc-14-1951-2020>.
- Dukhovskoy, D. S., and Coauthors, 2016: Greenland freshwater pathways in the sub-Arctic Seas from model experiments with passive tracers. *J. Geophys. Res. Oceans*, **121**, 877–907, <https://doi.org/10.1002/2015JC011290>.
- , I. Yashayaev, A. Proshutinsky, J. L. Bamber, I. L. Bashmachnikov, E. P. Chassignet, C. M. Lee, and A. J. Tedstone, 2019: Role of Greenland freshwater anomaly in the recent freshening of the subpolar North Atlantic. *J. Geophys. Res. Oceans*, **124**, 3333–3360, <https://doi.org/10.1029/2018JC014686>.
- Enderlin, E. M., I. M. Howat, S. Jeong, M. Noh, J. H. van Angelen, and M. R. van den Broeke, 2014: An improved mass budget for the Greenland ice sheet. *Geophys. Res. Lett.*, **41**, 866–872, <https://doi.org/10.1002/2013GL059010>.
- Fenty, I., and Coauthors, 2016: Oceans melting Greenland: Early results from NASA's ocean-ice mission in Greenland. *Oceanography*, **29**, 72–83, <https://doi.org/10.5670/oceanog.2016.100>.
- Forget, G., J.-M. Campin, P. Heimbach, C. N. Hill, R. M. Ponte, and C. Wunsch, 2015: ECCO version 4: An integrated framework for non-linear inverse modeling and global ocean state estimation. *Geosci. Model Dev.*, **8**, 3071–3104, <https://doi.org/10.5194/gmd-8-3071-2015>.
- Frajka-Williams, E., J. L. Bamber, and K. Våge, 2016: Greenland melt and the Atlantic meridional overturning circulation. *Oceanography*, **29**, 22–33, <https://doi.org/10.5670/oceanog.2016.96>.
- Gade, H. G., 1979: Melting of ice in sea water: A primitive model with application to the Antarctic ice shelf and icebergs. *J. Phys. Oceanogr.*, **9**, 189–198, [https://doi.org/10.1175/1520-0485\(1979\)009<0189:MOIISW>2.0.CO;2](https://doi.org/10.1175/1520-0485(1979)009<0189:MOIISW>2.0.CO;2).
- Goelzer, H., and Coauthors, 2020: The future sea-level contribution of the Greenland ice sheet: A multi-model ensemble study of ISMIP6. *Cryosphere*, **14**, 3071–3096, <https://doi.org/10.5194/tc-14-3071-2020>.
- Heuzé, C., A. Wählin, H. L. Johnson, and A. Münchow, 2016: Pathways of meltwater export from Petermann Glacier, Greenland. *J. Phys. Oceanogr.*, **47**, 405–418, <https://doi.org/10.1175/JPO-D-16-0161.1>.
- Inall, M. E., T. Murray, F. R. Cottier, K. Scharrer, T. J. Boyd, K. J. Heywood, and S. L. Bevan, 2014: Oceanic heat delivery via Kangerdlugssuaq Fjord to the south-east Greenland ice sheet. *J. Geophys. Res. Oceans*, **119**, 631–645, <https://doi.org/10.1002/2013JC009295>.
- Jackson, R. H., F. Straneo, and D. A. Sutherland, 2014: Externally forced fluctuations in ocean temperature at Greenland glaciers in non-summer months. *Nat. Geosci.*, **7**, 503–508, <https://doi.org/10.1038/ngeo2186>.
- , S. J. Lentz, and F. Straneo, 2018: The dynamics of shelf forcing in Greenlandic fjords. *J. Phys. Oceanogr.*, **48**, 2799–2827, <https://doi.org/10.1175/JPO-D-18-0057.1>.
- Jenkins, A., 1999: The impact of melting ice on ocean waters. *J. Phys. Oceanogr.*, **29**, 2370–2381, [https://doi.org/10.1175/1520-0485\(1999\)029<2370:TIOMIO>2.0.CO;2](https://doi.org/10.1175/1520-0485(1999)029<2370:TIOMIO>2.0.CO;2).
- , 2011: Convection-driven melting near the grounding lines of ice shelves and tidewater glaciers. *J. Phys. Oceanogr.*, **41**, 2279–2294, <https://doi.org/10.1175/JPO-D-11-03.1>.
- Johnson, H. L., A. Münchow, K. K. Falkner, and H. Melling, 2011: Ocean circulation and properties in Petermann Fjord, Greenland. *J. Geophys. Res.*, **116**, C01003, <https://doi.org/10.1029/2010JC006519>.

- Khazendar, A., and Coauthors, 2019: Author correction: Interruption of two decades of Jakobshavn Isbrae acceleration and thinning as regional ocean cools. *Nat. Geosci.*, **12**, 493, <https://doi.org/10.1038/s41561-019-0382-y>.
- Le Bras, I., F. Straneo, M. Muilwijk, L. H. Smedsrud, F. Li, M. S. Lozier, and N. P. Holliday, 2021: How much Arctic fresh water participates in the subpolar overturning circulation? *J. Phys. Oceanogr.*, **51**, 955–973, <https://doi.org/10.1175/JPO-D-20-0240.1>.
- Locarnini, M., and Coauthors, 2018: *Temperature*. Vol. 1, *World Ocean Atlas 2018*, NOAA Atlas NESDIS 81, 52 pp.
- MacCready, P., and W. R. Geyer, 2010: Advances in estuarine physics. *Annu. Rev. Mar. Sci.*, **2**, 35–58, <https://doi.org/10.1146/annurev-marine-120308-081015>.
- Mankoff, K. D., F. Straneo, C. Cenedese, S. B. Das, C. G. Richards, and H. Singh, 2016: Structure and dynamics of a subglacial discharge plume in a Greenlandic fjord. *J. Geophys. Res. Oceans*, **121**, 8670–8688, <https://doi.org/10.1002/2016JC011764>.
- McDougall, T. J., and P. M. Barker, 2011: Getting Started with TEOS-10 and the Gibbs Seawater (GSW) Oceanographic Toolbox. SCOR/IAPSO, 28 pp., [www.TEOS-10.org](http://www.TEOS-10.org).
- Moon, T., D. A. Sutherland, D. Carroll, D. Felikson, L. Kehrl, and F. Straneo, 2018: Subsurface iceberg melt key to Greenland fjord freshwater budget. *Nat. Geosci.*, **11**, 49–54, <https://doi.org/10.1038/s41561-017-0018-z>.
- Morlighem, M., and Coauthors, 2017: BedMachine v3: Complete bed topography and ocean bathymetry mapping of Greenland from multibeam echo sounding combined with mass conservation. *Geophys. Res. Lett.*, **44**, 11–51, <https://doi.org/10.1002/2017GL074954>.
- , M. Wood, H. Seroussi, Y. Choi, and E. Rignot, 2019: Modeling the response of Northwest Greenland to enhanced ocean thermal forcing and subglacial discharge. *Cryosphere*, **13**, 723–734, <https://doi.org/10.5194/tc-2018-214>.
- Mortensen, J., K. Lennert, J. Bendtsen, and S. Rysgaard, 2011: Heat sources for glacial melt in a sub-Arctic fjord (Godthåbsfjord) in contact with the Greenland Ice Sheet. *J. Geophys. Res.*, **116**, C01013, <https://doi.org/10.1029/2010JC006528>.
- , S. Rysgaard, J. Bendtsen, K. Lennert, T. Kanzow, H. Lund, and L. Meire, 2020: Subglacial discharge and its down-fjord transformation in West Greenland fjords with an ice mélange. *J. Geophys. Res. Oceans*, **125**, e2020JC016301, <https://doi.org/10.1029/2020JC016301>.
- Morton, B. R., G. I. Taylor, and J. S. Turner, 1956: Turbulent gravitational convection from maintained and instantaneous sources. *Proc. Roy. Soc. London*, **A234**, 1–23, <https://doi.org/10.1098/rspa.1956.0011>.
- Mouginot, J., and Coauthors, 2019: Forty-six years of Greenland Ice Sheet mass balance from 1972 to 2018. *Proc. Natl. Acad. Sci. USA*, **116**, 9239–9244, <https://doi.org/10.1073/pnas.1904242116>.
- Münchow, A., K. K. Falkner, and H. Melling, 2015: Baffin Island and West Greenland current systems in northern Baffin Bay. *Prog. Oceanogr.*, **132**, 305–317, <https://doi.org/10.1016/j.pocean.2014.04.001>.
- Noël, B., and Coauthors, 2018: Modelling the climate and surface mass balance of polar ice sheets using RACMO2-Part 1: Greenland (1958–2016). *Cryosphere*, **12**, 811–831, <https://doi.org/10.5194/tc-12-811-2018>.
- Nürser, A. J., and S. Bacon, 2014: The Rossby radius in the Arctic Ocean. *Ocean Sci.*, **10**, 967–975, <https://doi.org/10.5194/os-10-967-2014>.
- OMG Mission, 2020: Conductivity, Temperature and Depth (CTD) data from the ocean survey, version 0.1. OMG SDS, accessed 2 January 2020, <https://doi.org/10.5067/OMGEV-AXCTD>.
- Perner, K., M. Moros, O. H. Otterå, T. Blanz, R. R. Schneider, and E. Jansen, 2019: An oceanic perspective on Greenland's recent freshwater discharge since 1850. *Sci. Rep.*, **9**, 17680, <https://doi.org/10.1038/s41598-019-53723-z>.
- Rignot, E., I. Fenty, D. Menemenlis, and Y. Xu, 2012: Spreading of warm ocean waters around Greenland as a possible cause for glacier acceleration. *Ann. Glaciol.*, **53**, 257–266, <https://doi.org/10.3189/2012AoG60A136>.
- Rysgaard, S., and Coauthors, 2020: An updated view on water masses on the pan-west Greenland continental shelf and their link to proglacial fjords. *J. Geophys. Res. Oceans*, **125**, e2019JC015564, <https://doi.org/10.1029/2019JC015564>.
- Shepherd, A., and Coauthors, 2020: Mass balance of the Greenland Ice Sheet from 1992 to 2018. *Nature*, **579**, 233–239, <https://doi.org/10.1038/s41586-019-1855-2>.
- Slater, D. A., P. W. Nienow, T. R. Cowton, D. N. Goldberg, and A. J. Sole, 2015: Effect of near-terminus subglacial hydrology on tidewater glacier submarine melt rates. *Geophys. Res. Lett.*, **42**, 2861–2868, <https://doi.org/10.1002/2014GL062494>.
- , D. N. Goldberg, P. W. Nienow, and T. R. Cowton, 2016: Scalings for submarine melting at tidewater glaciers from buoyant plume theory. *J. Phys. Oceanogr.*, **46**, 1839–1855, <https://doi.org/10.1175/JPO-D-15-0132.1>.
- , F. Straneo, D. Felikson, C. M. Little, H. Goelzer, X. Fettweis, and J. Holte, 2019: Estimating Greenland tidewater glacier retreat driven by submarine melting. *Cryosphere*, **13**, 2489–2509, <https://doi.org/10.5194/tc-13-2489-2019>.
- Straneo, F., and C. Cenedese, 2015: The dynamics of Greenland's glacial fjords and their role in climate. *Annu. Rev. Mar. Sci.*, **7**, 89–112, <https://doi.org/10.1146/annurev-marine-010213-135133>.
- , and M. Muilwijk, 2021: Temperature and Salinity profiles from Upernavik Fjord, Northwest Greenland, from 2013 to 2019. Arctic Data Center, accessed 1 February 2021, <https://doi.org/10.18739/A2SJ19S1Q>.
- , R. G. Curry, D. Sutherland, G. S. Hamilton, C. Cenedese, K. Våge, and L. Stearns, 2011: Impact of fjord dynamics and glacial runoff on the circulation near Helheim Glacier. *Nat. Geosci.*, **4**, 322–327, <https://doi.org/10.1038/ngeo1109>.
- , and Coauthors, 2012: Characteristics of ocean waters reaching Greenland's glaciers. *Ann. Glaciol.*, **53**, 202–210, <https://doi.org/10.3189/2012AoG60A059>.
- , and Coauthors, 2013: Challenges to understanding the dynamic response of Greenland's marine terminating glaciers to oceanic and atmospheric forcing. *Bull. Amer. Meteor. Soc.*, **94**, 1131–1144, <https://doi.org/10.1175/BAMS-D-12-00100.1>.
- Sutherland, D. A., and R. S. Pickart, 2008: The East Greenland coastal current: Structure, variability, and forcing. *Prog. Oceanogr.*, **78**, 58–77, <https://doi.org/10.1016/j.pocean.2007.09.006>.
- , F. Straneo, and R. S. Pickart, 2014: Characteristics and dynamics of two major Greenland glacial fjords. *J. Geophys. Res. Oceans*, **119**, 3767–3791, <https://doi.org/10.1002/2013JC009786>.
- Swingedouw, D., and Coauthors, 2013: Decadal fingerprints of freshwater discharge around Greenland in a multi-model

- ensemble. *Climate Dyn.*, **41**, 695–720, <https://doi.org/10.1007/s00382-012-1479-9>.
- Tomczak, M., and D. G. B. Large, 1989: Optimum multiparameter analysis of mixing in the thermocline of the eastern Indian Ocean. *J. Geophys. Res.*, **94**, 16141–16149, <https://doi.org/10.1029/JC094iC11p16141>.
- van den Broeke, M. R., E. M. Enderlin, I. M. Howat, P. Kuipers Munneke, B. P. Y. Noël, W. Jan Van De Berg, E. Van Meijgaard, and B. Wouters, 2016: On the recent contribution of the Greenland ice sheet to sea level change. *Cryosphere*, **10**, 1933–1946, <https://doi.org/10.5194/tc-10-1933-2016>.
- Vermassen, F., and Coauthors, 2019: A reconstruction of warm-water inflow to Upernavik Isstrøm since 1925 CE and its relation to glacier retreat. *Climate Past*, **15**, 1171–1186, <https://doi.org/10.5194/cp-15-1171-2019>.
- Wood, M., and Coauthors, 2021: Ocean forcing drives glacier retreat in Greenland. *Sci. Adv.*, **7**, eaba7282, <https://doi.org/10.1126/sciadv.aba7282>.